A p53-dependent translational program directs tissue-selective phenotypes in a model of ribosomopathies

Gerald C. Tiu[1,2,3†], Craig H. Kerr[1,2†], Craig M. Forester[5,6], Pallavi S. Krishnarao[1,2], Hannah D. Rosenblatt[1,2], Nitin Raj[7], Olena Zhulyn[1,2], Margot E. Bowen[7], Leila Shokat[1,2], Laura D. Attardi[1,7], Davide Ruggero[4,5,8], Maria Barna[1,2*]

[1] Department of Genetics, Stanford University School of Medicine, Stanford, CA, USA

[2] Department of Developmental Biology, Stanford University, Stanford, CA, USA

[3] Stanford Medical Scientist Training Program, Stanford University, Stanford, California, USA

[4] Department of Urology, University of California, San Francisco, San Francisco, CA, USA

[5] Helen Diller Family Comprehensive Cancer Center, University of California, San Francisco, San Francisco, CA, USA

[6] Division of Pediatric Allergy, Immunology & Bone Marrow Transplantation, University of California, San Francisco, San Francisco, CA, USA

[7] Division of Radiation and Cancer Biology, Department of Radiation Oncology, Stanford University School of Medicine, Stanford,CA, USA

[8] Department of Cellular and Molecular Pharmacology, University of California, San Francisco, San Francisco, CA, USA

[†] These authors contributed equally to this work.

*Correspondence to: mbarna@stanford.edu

ABSTRACT

In ribosomopathies, perturbed expression of ribosome components leads to tissue-specific phenotypes, such as limb and craniofacial defects as well as bone marrow failure. What accounts for such tissue-selective manifestations and what role translation plays is poorly understood. Combining comprehensive mouse genetics and *in vivo* ribosome profiling, we observe limb patterning phenotypes in ribosomal protein (RP) haploinsufficient embryos and uncover corresponding selective translational changes of transcripts controlling limb development. Surprisingly, either loss of p53, which is activated by RP haploinsufficiency, or augmented protein synthesis rescues these phenotypes. These findings are reconciled by the unexpected identification of p53 as a master regulator of protein synthesis, which specifically induces 4E-BP1 expression. 4E-BP1, a key regulator of gene expression at the translation level, facilitates selective changes in the translatome and thereby explains, at least in part, how RP haploinsufficiency may elicit specificity to gene regulation. These results provide an integrative model to explain how a tissue-specific phenotype may emerge from a mutation in a ribosome component.

ONE SENTENCE SUMMARY

A p53-4E-BP1 axis imparts translational remodeling associated with selective developmental phenotypes in an *in vivo* ribosomopathy model.

MAIN TEXT

Ribosomopathies are characterized by mutations in ribosome components that produce unexpected tissue-specific phenotypes. For example, Diamond Blackfan Anemia (DBA), which arises from haploinsufficiency of ~20 different essential RPs, converges upon a common set of poorly understood congenital birth defects that affect up to 50% of patients such as craniofacial, digit, and limb abnormalities, as well as selective impairment of erythroid differentiation, suggesting core ribosome dysfunction can lead to selective disease manifestations *(1, 2)*. Given the tissue specificity of ribosomopathy phenotypes, it is surprising that changes to translation have been largely unexplored within *in vivo* developmental contexts associated with RP haploinsufficiency. While a recent *ex vivo* cell culture study identified translational defects in hematopoietic cells upon knockdown of RPs mutated in DBA *(3)*, a multitude of other studies suggest that *in vivo* phenotypes underlying ribosomopathies can arise from the stress-induced transcription factor p53, through distinct mechanisms that sense defective ribosomes and activate p53 (see supplementary text) *(4–7)*. Stabilization of p53 is thought to contribute, at least in part, to ribosomopathies through transcriptional activation of genes canonically involved in regulating cell proliferation and apoptosis *(6)*. However, how such generic effects on cells lead to highly specific developmental phenotypes remains a paradox. Given these findings, it is unclear what roles p53-dependent and independent mechanisms play in the development of *in vivo* tissue-specific phenotypes associated with loss of function of a core ribosome component and what role translational regulation plays in this process.

RESULTS

Ribosomal protein haploinsufficiency leads to selective developmental phenotypes

To systematically delineate how haploinsufficiency of an essential RP leads to tissue-specific developmental phenotypes, we perturbed expression of the small subunit RP, Rps6 *(8, 9)*, in the developing mouse embryo*. Rps6* loss of function has served as a model to study ribosomopathies, as conditional *Rps6* hemizygosity within the hematopoietic compartment leads to erythroid phenotypes similar to that of other RPs found mutated in ribosomopathies such as DBA *(10)*. To investigate *Rps6* haploinsufficiency in an *in vivo* context, without affecting organismal viability, we turned to the developing limb bud, a well-established model system for studying tissue patterning and where defects emerge in ribosomopathies *(11)*. Limbs arise from a small bud of mesenchymal cells that includes chondrocyte progenitors, which give rise to all the skeletal elements of the limb covered by a surface ectoderm. The apical ectodermal ridge (AER) is a morphologically distinct ectoderm surrounding the distal tip of the limb bud that serves as an important signaling center that promotes limb outgrowth and survival of the underlying mesenchyme *(12)* (Fig. 1A). The basic vertebrate limb skeleton derives from a cartilaginous model: a single proximal long bone within the stylopod segment (humerus; femur), followed by two long bones within the zeugopod segment (radius, ulna; tibia, fibula) and then the distal autopod segment comprising of wrist or ankle, and digits (Fig. 1A). Using two distinct and well-established Cre lines driven by the *Prx1* promoter/enhancer *(13)* or the *Msx2* promoter *(14)*, we conditionally deleted one allele of *Rps6* in either the underlying limb mesenchyme or AER, respectively. Within the forelimb of $Prx1^{Cre};Rps6^{lox/+}$ embryos, a significant decrease of Rps6 was detected as early as stage E10.5 where Cre recombinase was broadly activated throughout the limb bud mesenchyme (Fig. 1K; fig. S1A) *(13)*. At E17.5, $Prx1^{Cre};Rps6^{lox/+}$ embryos demonstrated striking selective underdevelopment (hypoplasia) or loss (aplasia) of the anterior zeugopod element (the radius) compared to the ulna (28/28 limbs) in addition to scapular hypoplasia (28/28 limbs); hypoplasia/absence of the proximal humerus (28/28 limbs); and selective hypoplasia/absence of digits 1/2 (28/28 limbs), digit 4 (26/28 limbs), and digit 5 (28/28 limbs) marked by reduced phalangeal numbers, with digits 1 and 5 exhibiting the most

severe phenotypes (Fig. 1B-C; fig. S1B-C; table S1). Quantifying the ratio of radial ossification length to that of the ulna confirmed significant and penetrant radial aplasia in the *Prx1*^{Cre}*;Rps6*$^{lox/+}$ embryos compared to control (Fig. 1J). Surprisingly, we did not observe any phenotype when Rps6 was reduced in the AER (see *Msx2*^{Cre}*;Rps6*$^{lox/+}$; Fig. 1D,G; fig. S1D,G,J,M), revealing the cell type-specific effects of RP haploinsufficiency. Interestingly, the *Prx1*^{Cre}*;Rps6*$^{lox/+}$ phenotype is reminiscent of those found in DBA patients who can present with limb patterning defects including hypoplastic digit 1 and selective radial aplasia *(11, 15)*. The hindlimbs, on the contrary, displayed a much milder phenotype consisting of a hypoplastic digit 1 and a smaller, medially displaced patella (Fig. 1E-F; fig. S1E-F, H-I, K-L). However, the *Prx1*^{Cre} transgene is activated at a later developmental stage in the hindlimb relative to the forelimb, which could account for the milder phenotype. Indeed, when inactivating one allele of *Rps6* with *T*^{Cre}, which activates at an earlier stage of development, we observe hindlimb phenotypes including tibial hypoplasia/aplasia, oligodactyly, and hypoplasia/aplasia of the pelvis and femur analogous to what is observed in the *Prx1*^{Cre}*;Rps6*$^{lox/+}$ forelimbs (fig S2, table S1). Furthermore, the selective radial and digit phenotypes were observed as early as E12.5 by *in situ* hybridization against *Sox9*, the earliest marker of mesenchyme condensations, suggesting that these phenotypes result from defects in patterning prior to cartilage formation (Fig. 1H-I).

We hypothesized that the phenotypes may arise from either p53 activation or perturbed protein synthesis. Thus, we first asked whether p53 is activated in E10.5 *Prx1*^{Cre}*;Rps6*$^{lox/+}$ limb buds, approximately one day after Cre-mediated *Rps6* recombination in the limb mesenchyme. Indeed, we observed spatially homogeneous p53 activation and transcriptional upregulation of known p53 target genes *(16, 17)* (Fig. 1L-M; fig. S3A). This was accompanied by increased apoptosis and mildly decreased cell proliferation that were not spatially restricted within the limb bud mesenchyme (fig. S3B-E). Surprisingly, we also observed p53 activation in the ectoderm of *Msx2*^{Cre}*;Rps6*$^{lox/+}$ embryos (fig. S4), suggesting tissue specific responsiveness to Rps6 haploinsufficiency and p53 activation. Next, we measured changes in global protein

synthesis per cell by quantifying incorporation of O-propargyl-puromycin (OP-Puro) into nascent peptides of dissociated E10.5 limb mesenchymal cells (fig. S8A) *(18)*. We observed reduced OP-Puro incorporation in *Prx1*^{Cre}*;Rps6*$^{lox/+}$ versus control, indicating that protein synthesis is impaired in the developing limb bud upon Rps6 reduction (Fig. 1N). These data suggest that both p53 activation and defects in global protein synthesis underlie the observed limb patterning phenotypes upon Rps6 haploinsufficiency.

mTORC1 activation or loss of p53 rescue limb defects

We next turned to *in vivo* genetics to determine the contributions of decreased protein synthesis and/or p53 activation on the *Prx1*^{Cre}*;Rps6*$^{lox/+}$ limb phenotypes (Fig. 2A). First, we sought to genetically modulate global protein synthesis using one of the most well-described pathways that impacts translational control, the mTOR pathway *(19)*. mTOR signaling functions are distributed between at least two distinct mTOR protein complexes: mTORC1 and mTORC2. In particular, one of the major functions of mTORC1 signalling is controlling protein synthesis levels by phosphorylating key translational regulators, which subsequently leads to upregulation of cap-dependent protein synthesis (Fig. 2B) *(18–20)*. Therefore, to specifically activate mTORC1 in the limb, we conditionally inactivated the tuberous sclerosis complex (TSC), which specifically represses mTORC1 *(20, 21)*, by genetically deleting the TSC component *Tsc2* (fig. S5). Loss of *Tsc2* activates mTORC1 in developing limbs (fig. S5B) and strikingly rescues the *Rps6* haploinsufficiency patterning phenotype as exemplified by improved radial development in *Prx1*^{Cre}*;Rps6*$^{lox/+}$*;Tsc2*$^{lox/lox}$ compared to *Prx1*^{Cre}*;Rps6*$^{lox/+}$*;Tsc2*$^{+/+}$ limbs (Fig. 2C-F; fig. S5A), although overall limb size is still smaller. This phenotypic rescue in limb patterning is accompanied by a concurrent increase in protein synthesis as measured by OP-Puro incorporation in E10.5 limb buds (Fig. 2G). Loss of *Tsc2* did not influence *Rps6* expression nor does it abrogate the p53 activation induced by *Rps6* haploinsufficiency (Fig. 2H; fig. S5C). Furthermore, we

also observed phenotypic rescue in limb patterning but not full rescue of limb size when *Pten*, another upstream negative regulator of mTOR, is deleted in the developing limb bud (fig. S6). Taken together, these results suggest that perturbed translation may contribute to the developmental patterning phenotypes observed upon *Rps6* reduction.

Despite the rescue of the *Rps6* haploinsufficiency phenotype by mTORC1 activation and concomitant upregulation of global protein synthesis, we examined whether p53 activation also contributes to the limb phenotype (Fig. 3). We therefore crossed *Prx1*^{Cre}*;Rps6*$^{lox/+}$ mice into a p53 null background (*Trp53*$^{-/-}$; fig. S7) and observed that loss of p53 also rescues the limb phenotype, including radial aplasia and size (Fig. 3A-D; fig. S7A). As *Tsc2* deletion primarily restored limb patterning defects (Fig. 2), it is likely that changes in cell proliferation and apoptosis driven by p53 may contribute to limb size defects seen in *Prx1*^{Cre}*;Rps6*$^{lox/+}$*;Tsc2*$^{lox/lox}$ mice (fig. S3; fig. S5). However, we cannot exclude that protein synthesis is not completely restored to normal levels in *Prx1*^{Cre}*;Rps6*$^{lox/+}$*;Tsc2*$^{lox/lox}$ mice, which may also lead to incomplete rescue of limb size. Together these findings surprisingly show that either activation of the mTORC1 pathway with associated restoration of global protein synthesis or inactivation of p53 results in a genetic rescue of *Rps6* haploinsufficient patterning phenotypes *in vivo*.

These genetic findings raise the possibility that p53 activity and translational control may somehow be unexpectedly coupled in the context of RP haploinsufficiency. In support of this, past studies in cultured cells have suggested that p53 may regulate translation *(22)*, for example by suppressing mTORC1 activity by activating Sestrin, a negative regulator of mTORC1 *(23, 24)*. However, in the context of *Rps6* haploinsufficiency, we do not observe a difference in mTORC1 activity *in vivo* (fig. S9A-B). Therefore, we explored whether p53 accounts for the alterations in protein synthesis observed upon RP haploinsufficiency through a yet unknown mechanism (Fig. 3E). Strikingly, loss of p53 rescues the protein synthesis defect observed upon reduction of Rps6 in E10.5 limb buds as measured by OP-Puro incorporation (Fig. 3F). To determine whether p53 activation alone is sufficient to repress global protein

synthesis, we assayed the incorporation of the methionine analog L-Homopropargylglycine (HPG) into nascent peptides in primary mouse embryonic fibroblasts (MEFs) treated with p53 small molecule activators Nutlin-3a, which specifically blocks interaction of Mdm2 with p53, or doxorubicin (Doxo), which induces genotoxic stress *(25, 26)*. Nutlin-3a and doxorubicin treatment led to a decrease in global protein synthesis within 8 hours of treatment (Fig. 3G). Importantly, we did not observe a significant difference in apoptosis and only a modest decrease in cell proliferation after 8 h of Nutlin-3a treatment (fig. S8B-C). Collectively, these findings unexpectedly demonstrate that p53 is required to repress protein synthesis upon Rps6 reduction and that p53-dependent control of translation occurs through an unknown mechanism independent of mTORC1 pathway activation.

p53 drives translational changes upon Rps6 haploinsufficiency

To determine which transcripts are specifically perturbed on a genome-wide scale, we performed ribosome profiling directly on E10.5 *Rps6* haploinsufficient limb buds in a *Trp53*$^{+/+}$ or *Trp53*$^{-/-}$ background (Fig. 4A-B, fig. S10, fig. S11) *(27)*. Although standard ribosome profiling cannot detect alterations in global protein synthesis, this technique can pinpoint relative changes in the translation efficiency (TE) of specific transcripts *(28)*. We observed a large degree of translational changes upon Rps6 reduction (138 transcripts TE increased, 282 transcripts TE decreased) of which most changes are rescued by loss of p53 (Fig. 4A-B, fig. S11A,C, table S3). Interestingly, a smaller subset of differentially translated mRNAs was not dependent on p53 (64 transcripts TE increased, 8 transcripts TE decreased)(Fig. 4A-B, fig. S11B,D, table S4), which included p53 regulators and cytoplasmic RPs (see below).

Gene set enrichment analysis revealed that translationally repressed gene sets include those involved in limb development (Fig. 4C, table S5), corresponding to the observed phenotypes. Hence, the selective changes in translational control may account for the specificity in the limb patterning defects observed. For example,

transcripts in these gene sets whose decrease in TE is primarily due to reduction in ribosome footprints and not to changes in transcript levels included *Col2a1*, *Dicer1*, *Gli2*, and *Megf8* (Fig. 4D). *Col2a1* encodes for collagen type II alpha 1 chain, a component of the cartilage that lays the framework for skeletal development of most bones *(29)*. *Dicer1*, which encodes an RNase essential for miRNA maturation, is essential for proper limb maturation and survival of mesenchymal cells *(30)*. Furthermore, loss of *Gli2*, a component of the Sonic Hedgehog pathway, leads to shortened limbs with particular shortening of the radial bone *(31)*, while mutations in *Megf8* lead to limb developmental defects in humans *(32)*. In addition, consistent with the p53-dependence of the *Rps6* limb phenotype, translational repression of these selective transcripts involved in limb development are dependent on p53 (Fig. 4D; fig. S11C-D).

Translationally upregulated mRNAs were enriched in gene sets that included those containing cytoplasmic RPs (50 RPs, Fig. 4C-D; fig. S11B,D). Our *in vivo* results may thus represent a possible translational feedback mechanism to restore RP homeostasis when core RP expression is perturbed. In fact, translation of *Rps6* itself was upregulated (table S3-4), suggesting that the phenotype may in fact be more severe with a further decrease in RPS6 protein levels had it not been for this feedback mechanism. Furthermore, in contrast to the translationally repressed limb development genes that are p53-dependent, RP translational upregulation is p53-independent (Fig. 4D, fig. S11B,D). Upregulation of RP translation was particularly unexpected given that *ex vivo* studies demonstrated a marked decrease in RP translation after RP depletion *(3)*, suggesting that *in vivo* results may differ profoundly from cultured cells in their response to RP haploinsufficiency. We also observed p53-independent translational downregulation of the p53 negative regulator *Mdm4* (Fig. 4D, fig. S11B,D). Mdm4 cooperates with Mdm2 to suppress p53 activity *(33)*. Thus, translational suppression of *Mdm4* may serve as a post-transcriptional quality control sensor to activate p53 in the context of RP haploinsufficiency. Other p53-independent changes included

translational upregulation of the interferon-related gene, *Ifrd1,* and translational downregulation of the RING finger-containing protein, *Rnf10* (Fig. 4D, fig. S11B,D).

We validated our ribosome profiling results using sucrose gradient polysome fractionation and subsequent RT-qPCR on select, differentially translated transcripts from E10.5 *Prx1*^{Cre}*;Rps6*$^{lox/+}$ and *Rps6*$^{lox/+}$ limb buds (fig. S12). Upon Rps6 reduction, we observed a shift to lighter polysomes for transcripts whose TE decreased in the ribosome profiling (e.g., *Col2a1, Dicer1, Gli2, and Megf8*) and observed a shift towards heavier polysomes for transcripts whose TE increased in the ribosome profiling (e.g., RPs) (fig. S12B-C). Taken together, these data demonstrate that complex translational remodeling occurs upon *Rps6* haploinsufficiency that consists of a p53-dependent program associated with transcripts that correspond to phenotypic changes and a smaller p53-independent program that may mediate homeostatic responses to RP perturbations.

Next, we investigated what features may regulate differential translational sensitivity of transcripts to *Rps6* haploinsufficiency. Previous studies have demonstrated that *cis*-features such as ORF length and 5'UTR structuredness contribute to translational control *(34)*. Indeed, we find that translationally repressed transcripts upon Rps6 reduction have longer ORFs compared to the pool of unchanging transcripts whereas transcripts that are upregulated in translation have shorter ORFs (Fig. 4E, fig. S13A). Additionally, repressed transcripts have more structured 5'UTRs whereas upregulated mRNAs tend to have less structured 5'UTRs (Fig. 4E). Notably, the p53-dependent, translationally repressed limb developmental genes *Col2a1*, *Dicer1*, *Gli2*, and *Megf8* have long ORF lengths and highly structured predicted 5'UTRs with the *Col2a1* 5'UTR ranking in the top 13th percentile (table S6).

Given these observations, we asked whether the 5'UTRs of differentially translated mRNAs are sufficient to drive translational change. To this end, we took advantage of limb micromass cultures as a well-established model system to study limb mesenchyme and cartilage formation that mimics many of the *in vivo* steps of cellular differentiation (Fig. 4F) *(35)*. In comparison to two control 5'UTRs taken from

transcripts whose translation was unaffected by RP haploinsufficiency (*Pkm* and *Cnot10*), we observed reduced reporter activity driven by the 5'UTRs of translationally repressed transcripts including *Col2a1*, *Mdm4*, *Gli2, Megf8,* and *Rnf10* in *Prx1*^{Cre}*;Rps6*$^{lox/+}$ limb micromass cultures (Fig. 4G). These results are in agreement with our ribosome profiling and polysome RT-qPCR data and suggest that 5'UTRs may drive the translational regulation of these genes. An exception was found for the 5'UTR of Ifrd1, which showed a profound decrease in activity whereas its TE increased in ribosome profiling (fig. S13B). By contrast, RP transcripts did not show a significant change in luciferase activity (*Rps19, Rps14, Rpl18a*) (Fig. 4G) despite being translationally upregulated in the ribosome profiling and polysome gradient experiments. These data suggest that the 5'UTRs of RP transcripts are not the sole contributing factors that determine their translational response to RP haploinsufficiency. Overall, these findings demonstrate that 5'UTRs are important *cis*-regulatory elements that may contribute, in part, to differential translational sensitivity for a subset of transcripts to RP haploinsufficiency.

p53 modulates translational control by upregulating 4E-BP1 expression

We next sought to determine mechanistically how RP haploinsufficiency leads to widespread yet specific p53-dependent translational remodeling (Fig. 5A). Upon Nutlin-3a/doxorubicin treatment, primary cells displayed reduced global protein synthesis only after 4 h post-treatment, suggesting that intermediate steps likely occur between p53 activation and translational repression (fig. S14B). Thus, we investigated whether these translational changes depend on p53's transactivation activity, and indeed Nutlin-3a/doxorubicin treatment in MEFs expressing the p53 transactivation dead mutant *Trp53*$^{LSL\text{-}25,26,53,54/LSL\text{-}25,26,53,54}$ *(Trp53*$^{QM/QM}$*)(17)* did not lead to a reduction in protein synthesis (Fig. 5B; fig. S14A), suggesting that p53-dependent translational repression requires its transactivation activity. We therefore asked what p53 transcriptional targets beyond those previously described may be responsible for these

translational changes. Strikingly, we found that mRNA and protein expression of *Eif4ebp1* (4E-BP1), which encodes a master regulator of cap-dependent translation, is induced upon reduction of Rps6 in embryonic limbs in a p53-dependent manner (Fig. 5C-D, fig. S15). We did not observe this with the closely related homolog, *Eif4ebp2* (Fig. 5D). In addition, loss of p53 abrogates 4E-BP1 upregulation upon *Rps6* haploinsufficiency, further supporting that p53 transcriptionally activates *Eif4ebp1* expression (Fig. 5C; fig. S15D-E). Intriguingly, *Eif4ebp1* upregulation was not detected upon Rps6 reduction in the AER where limb phenotypes were not observed despite p53 activation in these cells (Fig. 1D,G; fig. S4B), suggesting that there may be additional tissue-specific regulatory mechanisms governing *Eif4ebp1* expression.

Re-analyzing our previously generated genome-wide p53 ChIP-Seq data *(36)* revealed a ~0.4 kb region in the first exon of *Eif4ebp1* containing a putative p53 binding site, which was validated by ChIP-qPCR and specific to *Eif4ebp1* but not to *Eif4ebp2* (Fig. 5E; fig. S14C-D). When cloned into a luciferase reporter construct (fig. S14E), this region was sufficient to drive expression of luciferase upon p53 activation (Fig. 5F). Mutation of the core p53 binding sequence (*Eif4ebp1*$_{CATG\text{-}AGCT}$) abolished p53-dependent luciferase activity (Fig. 5F), revealing a genuine *cis*-regulatory element responsible for p53-dependent induction of *Eif4ebp1*.

The primary function of 4E-BP1 is to repress the major cap-binding protein, eukaryotic initiation factor 4E (eIF4E). eIF4E is rate limiting for the translation of select mRNAs, including those with specific sequences or structures within their 5'UTRs. For example, highly structured 5'UTRs are more sensitive to eIF4E dosage as it enhances the unwinding of RNA secondary structures during ribosome scanning by eIF4A *(37)*. In addition, distinct sequences in the 5'UTR of selective mRNAs such as the cytosine rich motif (CERT) also confer specificity to eIF4E activity *(38)*. Thus, increased expression of 4E-BP1 inhibits the formation of the eIF4E translation initiation complex and will thereby alter the translation of eIF4E-sensitive transcripts. To functionally test whether p53 activation leads to 4E-BP1-mediated cap-dependent translational repression, we performed cap-binding assays and observed enhanced binding of 4E-BP1 to eIF4E

and concomitantly reduced eIF4G that positively upregulates cap-dependent translation when bound to eIF4E in Nutlin-3a-treated cells (Fig. 5G). In addition, Nutlin-3a treatment did not appear to perturb cap-independent translation (fig. S16A). We next measured whether p53-dependent repression of global protein synthesis requires *Eif4ebp1* expression by depleting 4E-BP1 (fig. S16B-C). As 4E-BP1 and 4E-BP2 are functionally redundant, we knocked-down both proteins to prevent compensation of 4E-BP1 by 4E-BP2 *(39, 40)*. Importantly, 4E-BP1/2 knockdown rescues to a large extent the global protein synthesis repression observed upon Rps6 reduction in *Prx1*^{Cre}*;Rps6*$^{lox/+}$ primary micromass cultures (Fig. 5H) and in Nutlin-3a treated cells (fig. S16D). This effect was mirrored when 4E-BP1 was knocked-down alone (fig. S16E). Although 4E-BP1 activity can be regulated via phosphorylation by the mTOR pathway *(41)*, no significant change in 4E-BP1 phosphorylation was observed in *Prx1*^{Cre}*;Rps6*$^{lox/+}$ embryonic limbs relative to wildtype (fig. S9) or after 8 h of Nutlin-3a treatment (fig. S16F).

To further understand if 4E-BP1 upregulation is a general phenomenon associated with depletion of core RPs, we knocked down RPs commonly mutated in ribosomopathies such as DBA and 5q- myelodysplastic syndrome, Rps19 and Rps14, in primary limb micromass cultures and assessed p53 activation and *Eif4ebp1* transcription. As with Rps6 reduction, we found that p53 is activated upon depletion of Rps19 or Rps14, which coincides with an increase in *Eif4ebp1* expression (Fig. 6). Together, these results suggest a common pathway via the p53-4EBP1-eIF4E axis by which selective changes in translation occur upon ribosome perturbation, including in the context of RPs directly mutated in ribosomopathies. Although these assays were carried out in limb mesenchyme, it will be of interest in the future to test whether activation of the p53-4EBP1-eIF4E axis is a common feature in all tissues affected in ribosomopathies, including the hematopoietic lineage.

DISCUSSION

Our work establishes that changes in translational control underlie RP haploinsufficiency and contribute to phenotype. These changes to the translatome at the genome-wide scale are selective and correlate with the nature of the observed phenotypes. Our findings further reconcile the previous rescue of RP haploinsufficiency phenotypes by loss of p53 *(4, 9, 10)* but surprisingly demonstrate a completely unexpected role of p53, beyond its canonical role in transcription, in mediating much of the translation program downstream of core RP haploinsufficiency. Mechanistically, we demonstrate that p53 can directly control the levels of 4E-BP1 expression, which thereby enables cells to remodel the cellular translatome and downregulate cap-dependent translation in response to RP haploinsufficiency. Translation is one of the most energetically expensive programs in the cell. By coupling alterations in the expression of essential RPs directly to cap-dependent translation via 4E-BP1, p53 ensures that a modified cellular translatome continues to support cellular growth and survival under suboptimal conditions.

How can perturbed expression of 4E-BP1 elicit tissue-specific defects? The 4E-BP1-eIF4E axis is a rate-limiting component of translation initiation, for certain transcripts with specific sequences and structures in their 5'UTRs that are particularly sensitive to eIF4E mediated translational regulation *(37, 38)*. As a result, p53 mediated induction of 4E-BP1 can lead to a translational program in which perturbed expression of select transcripts, which are differentially sensitive to eIF4E activity, may contribute to tissue specific phenotypes. This is likely highly dependent on the nature of the transcripts expressed within specific cellular and/or tissue contexts and would result in translational downregulation of specific mRNAs that manifests in tissue specific phenotypes. For example, in the limb upon *Rps6* haploinsufficiency, we observe p53-dependent translational repression of key limb developmental transcripts that correlate with the observed limb development phenotype that p53-dependent control of translation may play a broader biological role in processes such as the regulation of cancer, where the 4E-BP1-eIF4E axis and aberrant translational control is known to drive multiple aspects of cancer development *(38, 42)*. Despite activation of the tumor

suppressor p53 observed in ribosomopathies such as DBA *(4)*, patients with DBA also surprisingly present with a higher incidence of cancer including leukemia and osteogenic sarcoma *(43)*. One explanation for how this paradoxical increase in cancer risk occurs is that activation of p53 upon RP haploinsufficiency would select for cells that lose p53 and its capacity to repress eIF4E-mediated translation via 4E-BP1. Therefore, a direct link between p53 and 4E-BP1-eIF4E activity established in this study suggests that characterization of p53-dependent remodeling of translation is likely to yield greater insights and novel therapeutic strategies to target cancer and ribosomopathies. In particular, small molecules that modulate translation may reflect important therapeutics for this class of diseases.

MATERIALS AND METHODS

Mouse husbandry. All animal work was reviewed and approved by the Stanford Administrative Panel on Laboratory Animal Care (APLAC). The Stanford APLAC is accredited by the American Association for the Accreditation of Laboratory Animal Care (AAALAC). All mice used in the study were housed at the Research Animal Facility (RAF) and at the SIM-1 Barrier Facility at Stanford University. Mice were maintained on mixed backgrounds and the following previously described alleles were used: *Rps6*^{lox} *(8)*, *Prx1*^{Cre} *(13)*, *Msx2*^{Cre} *(14)*, *Pten*^{lox} *(44)*, *Tsc2*^{lox} *(45)*, *Trp53*^{null} *(46)*, *T*^{Cre} *(47)*, and *Rosa*$^{mTmG/+}$ *(48)*. *Rps6*^{lox} mice were generously provided by George Thomas (IDIBELL). *Pten*^{lox} and *T*^{Cre} mice were generously provided by Zijie Sun and Mark Lewandoski, respectively. *Prx1*^{Cre}, *Msx2*^{Cre}, and *Tsc2*^{lox} mice were obtained from the Jackson Laboratories. Genotyping was performed using standard PCR protocols using primers described in aforementioned publications or on the Jackson Laboratories website. Common *Cre* primers were used to genotype *Cre* lines (http://mgc.wustl.edu/protocols/pcr_genotyping_primer_pairs). The following primers were used for *Rps6*^{lox} genotyping: Rps6lox_1 GCTTCTACTTCTAAGTCTGAGTCCAGTC, Rps6lox_2 TCCTGCCGAGAAAGTATCCATCATG, and Rps6lox_3 CTGCAGCCTTTTCTTTTAGCATACCTG. Mice for a given experiment were colony-matched. Mouse embryos for a given experiment were somite matched. Mouse embryos were harvested at E10.5, E11.5, E12.5, E13.5, and E17.5.

Cell Lines. Primary MEFs were derived from E13.5 mouse embryos using standard protocols and cultured under standard conditions in DMEM supplemented with 2 mM L-glutamine and 10% fetal bovine serum (FBS). Cells were used for experiments at passages 2-5. Both NIH3T3 and C3H10T1/2 cells were purchased from the American Type Culture Collection and grown under standard conditions in DMEM supplemented with 10% FBS and 2 mM L-glutamine. Cells were passaged 1:6 roughly every 4-5 days. All cell lines used in this study were mycoplasma-free.

Skeleton and cartilage staining. Bone and cartilage staining of E17.5 embryos were performed as per standard methods. Skeletal images were acquired using a Zeiss SteREO Discovery.V8 microscope and a Zeiss AxioCam MRc5 camera with an external standard as scale. Skeletal elements were measured using the ImageJ Fiji plug-in with genotypes blinded upon measurement.

Separation of limb ectoderm and mesenchyme. Forelimb buds of E11.5 embryos were dissected in 1×PBS. Dissected limb buds were then digested in 3% Trypsin in 1×PBS for 25 min at 4°C with gentle shaking. Trypsin digestion was quenched by moving the limb buds to 10% FBS in PBS. The limb buds were then gently vortex for 15 seconds to dislodge the mesenchymal and ectodermal layers. The ectodermal jackets were further removed from the individual limb buds under a dissecting microscope. Samples were stored at -80°C until use.

***In situ* hybridization.** *In situ* hybridization for *Sox9* at E12.5 was performed as per standard protocols *(49)* with modifications to achieve good probe penetration and signal. Digoxigenin (DIG) labeled RNA probes were generated from *XhoI* linearized T3 promoter *Sox9* plasmid (gift from Chi-Chung Hui, U Toronto). Fixed and rehydrated embryos were treated with 20 µg/mL proteinase K in PBS+0.1% Tween-20 (PBST) for 35 minutes at room temperature. After post-fixation and subsequent washes, embryos were incubated overnight at 70°C with hybridization mix containing 0.5 µg/mL denatured DIG-labeled probe. After washes and pre-blocking, embryos were incubated overnight at 4°C with 1:2000 alkaline phosphatase-conjugated anti-DIG antibodies (Sigma/Roche, 11093274910). After washes and prior to development, embryos were washed 2x20 min with 100 mM NaCl, 100 mM Tris-HCl pH 9.5, 50 mM $MgCl_2$, 0.1% Tween-20, 2 mM levamisole. Embryos were then developed with BM Purple AP substrate (Sigma/Roche, 11442074001) at 4°C for >1 day until adequate signal to noise ratio was achieved. The reaction was then subsequently inactivated, post-fixed, and stored. Embryos were then imaged with a Leica MZ16 FA microscope with a Leica DFC480 camera with an external standard used for scale.

Vectors and *in vitro* transcription. For generation of 5'UTR reporter constructs, sequences were obtained from ENSEMBL and isoforms were chosen based on alignment to the RNA sequencing results presented herein. 5'UTR gene fragments were synthesized (Twist Biosciences) and cloned immediately upstream of a Firefly luciferase gene encoded in pGL3-FLB (Leppek *et al.* unpublished). Each 5'UTR-*Fluc* construct was PCR amplified using primers flanking the 5'UTR and *Fluc* gene and incorporating a T7 RNA polymerase promoter at the 5' end. PCR amplicons were column purified (NEB, T1030) and used as a template for *in vitro* transcription reactions with a mMESSAGE mMACHINE® T7 Transcription Kit (Ambion, AM1344) followed by the addition of a poly(A) tail using a Poly(A) Polymerase Tailing Kit (Lucigen, PAP5104H). For HCV-IRES reporter RNA, the linearized vector pRF-HCV was used as a template. *In vitro* synthesized capped and poly(A) tailed RNA was purified using PureLink

RNA Mini Columns (Thermo Fisher, 12183020). RNA integrity was confirmed via denaturing agarose gel electrophoresis.

For testing p53 transcriptional activity, a 423 bp gene fragment of *Eif4ebp1* was amplified from genomic DNA of primary mouse embryonic fibroblasts and cloned in lieu of the minimal promoter sequence within pGL4.23[*luc2/miniP*]. All constructs were sequence verified.

siRNA-mediated knockdowns. NIH3T3 cells were plated at a density of 1.0×10^5 cells/well in a 6-well plate and allowed to attach for at least 6 h at 37°C. Cells were washed with 1×PBS before being transfected with 25 nM of non-targeting control siRNA or siRNA target against 4E-BP1 and 4E-BP2 (Dharmacon) using Dharmafect Reagent I (Dharmacon, T-2001) as per manufacturer's protocol. Cells were incubated for 12 h at 37°C in antibiotic-free media. Following incubation, the siRNA-containing media was replaced with complete DMEM media (as described above) and cells were treated with either DMSO, Nutlin-3a, or Doxorubicin.

For siRNA treatment in micromass limb cultures, limbs from E11.5 embryos were dissected and cells dissociated as described. Subsequently, 1.5×10^6 cells were reverse transfected with 25 nM siRNA as per manufacturer's protocol using Dharmafect I (Dharmacon, T-2001) in Limb micromass media and plated in a 96-well plate. Cells were incubated for 20 h before use in subsequent experiments. Note that siRNA knockdowns of Rps19 and Rps14 were performed in micromass cultures derived from wildtype *C57BL/6J* mice.

RT-qPCR quantification of RNA expression. RNA from embryonic limbs or cell culture was extracted with TRIzol (Thermo Fisher, 15596026) as per manufacturer's protocol followed by DNase I treatment for 30 min at 37°C. RNA was then purified via Zymo RNA Clean & Concentrator columns (Zymo Research). Subsequently, 100 ng of RNA was used for first strand cDNA synthesis using the iScript Supermix (Bio-rad, 1708841). cDNA was diluted 18-fold and 4 µL was used in a reaction for SYBR green detection with SsoAdvanced SYBR Green supermix (Bio-Rad, catalog no. 1725270) on a CFX384 machine (Bio-rad). All primer sequences are available in table S2.

Western blots. Equal amounts of protein were resolved on either a 15% or a 4-20% Tris-glycine gradient SDS-PAGE gel and transferred to a polyvinylidene difluoride Immobilon-FL membrane (PVDF; Bio-rad). Membranes were blocked for 30 min at room temperature with 5% BSA in TBST (50 mM Tris, 150 mM NaCl, 1% Tween-20, pH 7.4). Blots were incubated for 24 h at 4°C with the following primary antibodies: mouse anti-GAPDH (Cell Signalling, 97166), mouse anti-actin (Cell Signalling, 3700S), rabbit anti-Rps6 (Cell Signalling, 2217L), rabbit anti-4E-BP1 (Cell Signalling, 9644S), rabbit anti-phopsho-ULK1(Ser757)(Cell

Signalling, 6888T), rabbit anti-phospho-AKT(Ser473) (Cell Signalling, 9271S), rabbit anti-phopsho-4E-BP1(Ser65) (Cell Signalling, 9451S), rabbit anti-p53 (Leica Biosystems, CM5), rabbit anti-TSC2 (Cell Signalling, 4308T), rabbit anti-eIF4G (Cell Signalling, 2498S), mouse anti-eIF4E (BD Transduction, 610269). All antibodies were used at a dilution of 1:1000 in 5% BSA-TBST, unless stated otherwise. Membranes were washed 3 times for 5 min in TBST before incubation for 1 h at room temperature with secondary antibodies: donkey anti-mouse (1:5000; GE Healthcare, NA931-1ML), or donkey anti-rabbit (1:5000; GE Healthcare, NA934-1ML) coupled to Horseradish Peroxidase. Membranes were then washed 3 times for 5 min in TBST before detection using Clarity Western ECL Substrate (Bio-rad, 170-5061) and imaging on a ChemiDoc MP (Bio-rad, 17001402). All blots were quantified using ImageJ v2.0.0.

Micromass cultures and RNA transfection luciferase assays. E11.5 mouse limbs were harvested in DMEM/F12, no phenol red, 10% FBS, pen/strep. Cells were then dissociated in Dissociation Buffer (1% trypsin in HBSS without Ca^{+2} or Mg^{+2}) and incubated for 30 min at 37°C. Single-cell suspensions were obtained by quenching the dissociation with Limb Media (DMEM/F12 HEPES, 10% FBS) and passing through a cell strainer. Cells were then pelleted and resuspended in Limb Media. Next, 1.0×10^5 cells were co-transfected with capped and poly(A)-tailed Fluc (100 ng) and Rluc reporter RNAs (10 ng) using Lipofectamine 2000 (Thermo Fisher, 11668-019) before seeding into a single well of a 96-well Nunclon Delta Microplate (Thermo Fisher, 167008). Cells were incubated for 6 h at 37°C before being harvested in 1× Passive Lysis Buffer and subjected to a Luciferase assay as described above. Resulting luciferase activities were first normalized to to the geometric mean of *Pkm* and *Cnot10* 5'UTR activitiesand then to wildtype micromass cultures.

DNA transfection luciferase assays. NIH3T3 cells were seeded at a density of 1.0×10^5 cells/well in a 6-well plate and incubated at 37ºC overnight. The following day cells were co-transfected with 2 µg of Fluc plasmid DNA and 20 ng of Rluc control plasmid (pRL) per well using Lipofectamine 2000 (Thermo Fisher, 116688-019) and incubated for 16 h at 37ºC. Cells were then treated with either DMSO, Nutlin-3a (10 µM), or Doxorubicin (0.2 µg/mL) for 8 h. Cells were harvested and lysed in 50 µL of 1×Passive Lysis Buffer. Lysate was cleared of debris by centrifugation at 10,000 RCF for 5 min, and 20 µL of resulting supernatant was used to measure luciferase activity with the Dual-Luciferase Reporter Assay System (Promega, E1980) on a GloMax-Multi plate reader (Promega).

P53 transactivation domain mutated MEFs. MEFs were derived from previously generated knock-in mice expressing p53 wild-type ($Trp53^{LSL\text{-}WT/LSL\text{-}WT}$) or $Trp53^{QM/QM}$

(*Trp53*$^{LSL-25,26,53,54/LSL-25,26,53,54}$) mutant*(17)*. In these MEFs, expression of both *Trp53* alleles is silenced through upstream transcriptional stop element flanked by *loxP* recombination sites. To reactivate p53 expression, MEFs were infected with adenoviruses expressing Cre recombinase (Ad5 CMV-Cre) or empty virus (Ad5-CMV-Empty) as control at an approximate multiplicity of infection of 100. Viruses were purchased from University of Iowa Viral Vector Core Facility. Infected cells were cultured for 48 hours at 5% CO2, 37ºC before initiating drug treatments and HPG assay. Cells were treated with 0.2 µg/ml doxorubicin or 10 µM Nutlin-3a for indicated times (see below). High efficiency of recombination (>90% cells) was confirmed by immunostaining of p53. P53 stabilization upon doxorubicin and Nutlin-3a treatment was confirmed by Western blotting using p53 CM5 antibody (Leica Biosystems).

Chromatin immunoprecipitation qPCR. MEFs were grown in DMEM containing 10% FCS and seeded at 7 x 10^6 cells per 10 cm dish one day prior to the ChIP experiment. After treatment with 0.2 µg/ml doxorubicin for 6h, cells were harvested to prepare chromatin for immunoprecipitation using p53 polyclonal antibodies (NCL-L-p53-CM5p; Leica Biosystems). ChIPs were performed essentially as described previously *(36)*. Chromatin-immunoprecipitated DNA was quantified by qPCR using SYBR Green and a 7900HT Fast Real-Time PCR machine (Applied Biosystems) and primers specific for *Eif4ebp1*. The signals obtained from the ChIP were analyzed by the percent input method.

Cap-binding assays. NIH3T3 cells were seeded at a density of 1.0×10^6 in 10 cm tissue culture plates and incubated overnight at 37ºC. Cells were then treated with DMSO, Nutlin-3a (10 µM), or Doxorubicin (0.2 µg/mL) for 8 h. Subsequently, cells were harvested and washed twice with ice cold 1×PBS before being lysed for 30 min on ice with occasional agitation in Cap Lysis Buffer (10 mM Tris-HCl pH 7.5. 140 mM KCl, 4 mM $MgCl_2$, 1 mM DTT, 1 mM EDTA, 1% Nonidet P-40) supplemented with protease and phosphatase inhibitor for 30 min on ice with occasional agitation. Lysates were cleared via centrifugation at 10,000 RCF for 15 min at 4ºC. Resulting supernatants were collected and protein concentration was determined using a BCA assay (Thermo Fisher). 250 µg of protein was pre-cleared using 50 µL of agarose beads (Jena Biosciences, AC-100S) in Cap Lysis Buffer for 30 min at 4ºC with rocking. Next, the beads were pelleted at 1000 RCF and the supernatant was added to 50 µL of γ-aminophenyl-m7GTP (C10-spacer)-agarose beads (Jena Biosciences, AC-155S) in Cap Lysis Buffer overnight at 4ºC

with rocking. Supernatant was removed and the beads were washed twice with Cap Lysis Buffer followed by 1×PBS. Beads were then resuspended in 100 µL of 1× SDS loading buffer and boiled for 5 min. 25 µL of each sample was used for SDS-PAGE and Western blot analysis for eIF4E, eIF4G, and 4E-BP1.

Cell proliferation and apoptosis assays. Cell proliferation and apoptosis levels were measured using EdU (5-ethynyl-2´-deoxyuridine) incorporation and Annexin V staining, respectively. Briefly, 1.0×10^5 NIH3T3 cells were seeded in a 6-well plate and incubated overnight at 37ºC. The following day cells were treated with DMSO or Nutlin-3a (10 µM) for 4 or 8 h. For proliferation measurements, one hour before incubation was complete, cells were treated with 10 µM EdU using a Click-iT EdU Alexa Fluor 488 flow Cytometry Assay Kit (Thermo Fisher, C10425) and processed as per manufacturer's instructions. For apoptosis measurements, cells were harvested, washed twice with Cell Staining Buffer, and labeled using a FITC Annexin V and propidium iodide staining kit as per manufacturer's protocol (BioLegend, 640914). Both EdU- and Annexin V-labeled samples were analyzed on a LSRII flow cytometer (BD Biosciences) using software packages CellQuest and FlowJo v10.

Immunofluorescence on cryosections. Immunofluorescence on cryosectiosns was performed per standard protocols. Mouse embryos were dissected and fixed in ice-cold 4% PFA for 1 hour, washed four times with PBS + 0.1% Tween-20, equilibrated in 30% sucrose 0.1M potassium phosphate buffer, pH 7.4, embedded in O.C.T., and stored at -80ºC. Embryos were sectioned transversely into 12 um thick sections using a Leica cryostat, and frozen on slides at -80ºC until use. For immunofluorescence staining, all washes and incubations were done using blocking buffer (PBS with 1% goat serum and 0.1% Triton X-100). Sections were blocked for 1 hr in blocking buffer, incubated in primary antibody overnight at 4C, washed three times, incubated for 1 hr at room temperature with secondary antibody, and washed three more times before mounting. Primary antibodies were used at the following concentrations: 1:200 Leica anti-p53 (CM5P-L), 1:500 Sigma anti-phospho-Histone H3 (06-570), 1:600 Cell Signalling Technology Cleaved Caspase-3 (9661S). Goat anti-rabbit AF568 secondary from Life Technologies (A11036) was used for all slides at 1:500. Slides were imaged using a Zeiss EC 10x Plan-Neofluar Ph1 objective (NA = 0.3), and acquired using a CSU-X1 UltraVIEW Spinning disc with a Hamamatsu EM-CCD camera and Volocity software. Slides comparing the same antibodies were

imaged using consistent imaging settings and processing. For phospho-Histone H3 quantification, total cell count in the limb bud from multiple embryos was quantified from DAPI staining with Spot Counter in ImageJ, and pHistone3 positive cells were counted manually. Images are representative of average percentages of pHistone3 cells in Prx and WT sections.

Measurement of global protein synthesis. Briefly, O-propargyl-puromycin (OP-Puro) labeling of embryonic limbs was done as follows. E10.5 embryos were dissected in filming media (DMEM/F12, no phenol red, 10% FBS). Forelimbs were removed and dissociated in Dissociation Buffer (1% trypsin in HBSS without Ca^{+2} or Mg^{+2}) for 15 min at 37°C. Resuspended forelimb cells were used for downstream labeling and analysis. For OP-Puro or L-homopropargylglycine (HPG) labeling of cultured cells, primary MEFs or NIH3T3 cells were seeded at a density of 1.0×10^5 cells/well in a 6-well plate and allowed to attach overnight. The following day, cells were treated with DMSO, Nutlin-3a (10 μM), or Doxorubicin (0.2 μg/mL) before metabolic labeling. For OP-Puro incorporation, cells were labeled with 20 μM of OPP in DMEM plus drug for 30 min at 37°C. For HPG labeling, two hours before each timepoint, cells were methionine starved in Met dropout media (DMEM supplemented with 10% dialyzed FBS, 25mM L-cysteine, 2mM L-glutamine, no methionine) for 45 min at 37°C. Cells were then labeled with 50 μM HPG (Thermo Fisher, C10186) or 50 μM L-Met (control) for 1 h at 37°C. Following metabolic labeling, cells were harvested and washed with twice 1×PBS. Cell pellets were resuspended in Zombie Violet Live-Dead Stain (1:500 in PBS; BioLegend, 423113) and incubated for 15 min in the dark. Cells were then washed with Cell Staining Buffer (0.1% NaN_3, 2% FBS in HBSS) before being fixed in 1% PFA for 15 min on ice. Subsequently, cells were permeabilized overnight at 4°C in Perm Buffer (0.1% Saponin, 0.1% NaN_3, 3% FBS in PBS). The next day, cells were washed twice with Cell Staining Buffer (without 0.1% NaN_3), labeled with an Alexa Fluor 555 Picolyl Azide dye (Thermo Fisher, C10642) and incubated for 30 min at room temperature in the dark. Labeled cells were washed and resuspended in Cell Staining Buffer before being analyzed on a LSRII flow cytometer (BD Biosciences) and using software packages CellQuest and FlowJo v10.

Sucrose density gradients and RT-qPCR.

E10.5 mouse embryonic limbs were harvested in cold HBSS (Thermo Fisher, 14025-076) containing 100 μg/ml cycloheximide (CHX). Limb pairs from 3-4 embryos of a given genotype were pooled and lysed via vigorous pipetting and 30 minute incubation at 4°C in 175 μL lysis

buffer (20 mM Tris-HCl pH 7.5, 150 mM NaCl, 15 mM $MgCl_2$, 1 mM DTT, 8% glycerol, 1% Triton X-100, 100 µg/ml CHX (Sigma-Aldrich, C7698-1G), 200 U/mL SUPERase RNase Inhibitor (Thermo Fisher, AM2696), 20 U/ml Turbo DNAse (Thermo Fisher, AM2238), and 1X Halt Protease and Phosphatase Inhibitor Cocktail (Thermo Fisher, 78442). Samples were centrifuged at 1,300xg, 5 min and 10,000xg, 5 min to remove cell debris. Samples were then layered onto a 15-45% sucrose gradient or 25-50% sucrose gradient containing 20 mM Tris-HCl pH 7.5, 100 mM NaCl, 15 mM $MgCl_2$, and 100 µg/ml CHX. 15-45% gradient was made on a Biocomp Model 108 Gradient Master. 25-50% gradient was made by sequentially freezing at -80°C a 5-step gradient (50%, 43,75%, 37.5%, 31.25%, 25% sucrose). Samples layered on gradients were spun on a Beckman SW-60 rotor at 35,000 RPM, 2.5 h, 4°C. After centrifugation, gradients were fractionated using a Density Gradient Fraction System (Brandel, BR-188). To normalize for fraction volume in subsequent RT-qPCR experiments, 100 pg of *in vitro* transcribed RNA containing *Renilla* and *Firefly* luciferase (*in vitro* transcribed from the pRF-HCV vector) were added to each fraction. Equal volumes of fractions were then pooled as described in the text. RNA was then extracted by mixing samples with Acid-Phenol:Chloroform, pH 4.5 (with IAA, 125:24:1) (Thermo Fisher, AM9722), incubating at 65°C, 5 min, and subsequent centrifugation at 21,000xg, 10 min, RT. The aqueous phase was obtained, mixed 1:1 with 100% ethanol, and further purified using the RNA Clean & Concentrator-5 kit (Zymo Research, R1013). Samples were treated 30 minutes with TURBO DNase per manufacturer protocol (Thermo Fisher, AM2238), and subsequently purified again using the RNA Clean & Concentrator-5 kit. Next, 20 ng of RNA was used for first strand cDNA synthesis using the iScript Supermix (Bio-rad, 1708841). cDNA was diluted 20-fold and 4 µL was used in a reaction for SYBR green detection with SsoAdvanced SYBR Green supermix (Bio-Rad, catalog no. 1725270) on a CFX384 machine (Bio-rad). All primer sequences are available in table S2.

For analysis, the candidate transcript qPCR Ct value in each pooled fraction was normalized to that of the spike-in *in vitro* transcribed *Renilla* luciferase RNA. Normalized Ct values were converted from log to linear space, multiplied by the number of fractions combined per pool, and then normalized to the sum total across all pooled fractions for a given sample. These values were compared between genotypes for each fraction using a paired, two-tailed t-tests with samples paired based on day of collection and somite count.

Ribosome profiling of embryonic limb buds. Ribosome profiling was performed as described before*(50)* with modifications. Details are described below. E10.5 mouse embryonic limbs were

harvested in cold HBSS (Thermo Fisher, 14025-076) containing 100 µg/ml cycloheximide (CHX). Choice of RNase was particularly important given that low input samples from a pair of E10.5 embryonic limbs were used. Although RNase I offers better codon resolution than RNase A/T1, RNase I has been shown to degrade ribosomes when used in high concentrations relative to input RNA whereas RNase A and T1 better maintain ribosome integrity at a greater range of concentrations despite only cutting single stranded RNA at C/U and G, respectively*(51)*. Given that E10.5 embryonic limbs yield low amounts of RNA, RNase A and T1 were used to prevent excess ribosome degradation.

Embryonic heads were collected for subsequent genotyping. Limb pairs from each embryo were lysed via vigorous pipetting and 30 minute incubation at 4°C in 215 µL buffer A (20 mM Tris-HCl pH 7.5, 150 mM NaCl, 15 mM $MgCl_2$, 1 mM DTT, 8% glycerol, 1% Triton X-100, 100 µg/ml CHX (Sigma-Aldrich, C7698-1G), 20 U/ml Turbo DNAse (Thermo Fisher, AM2238), and Complete Protease Inhibitor EDTA-free (Sigma-Aldrich, 11836170001). Lysates were cleared via sequential centrifugation at 1,300g, 5 min and 10,000g, 10 min at 4°C. For RNA input for RNA-Seq, 70 µL of lysate was diluted in 55 µL of water and stored at -80°C in 375 µL of TRIzol LS (Thermo Fisher, 10296010). For ribosome profiling, 120 µL of cleared lysate was treated with 0.5 µg RNase A (Thermo Fisher, AM2271) and 300 U RNase T1 (Thermo Fisher, EN0541) for 30 min, RT with gentle rocking. The reaction was stopped by the addition of 100 U SUPERase RNase Inhibitor (Thermo Fisher, AM2694). Ribosomes were enriched by adding 110 µL lysate onto 900 µL sucrose cushion buffer (1 M sucrose in buffer A containing 20 U/mL SUPERase RNase Inhibitor), and centrifuging in a TLA 120.2 rotor (Beckman) 70,000 rpm, 4 h, 4 °C. The ribosome pellet containing the ribosome footprinted Ribo-Seq library was resuspended in 500 µL TRIzol.

Library preparation was adapted from previous protocols*(50, 52)* and the ARTseq Ribosome Profiling Kit manual (Epicentre, Illumina). In summary, total RNA and ribosome footprints were extracted using the Direct-zol Micro Kit (Zymo, R2060) with in-column DNase I treatment. To have an adequate amount of RNA for subsequent steps, pairs of samples of the same genotype were pooled to generate a single replicate sample, brought up to 90 µL with water, and precipitated with 150 µL isopropanol overnight -80°C after addition of 10 µL 3 M NaOAc pH 5.5 and 1.5 µL 15 mg/mL GlycoBlue Coprecipitant (Thermo Fisher, AM9515). The samples were then centrifuged at 21,000g, 30 min, 4°C, supernatant was removed, and the RNA pellet was washed 500 µL cold 75% ethanol. Pellets were dried for 10 min, RT and resuspended in 15 µL nuclease free water. After extraction and precipitation, both ribosome

footprinting and total RNA samples were depleted of rRNA using the Ribo-Zero Gold rRNA Removal Kit (H/M/R) (Illumina, catalog no. MRZG126) with the modification that the 50°C incubation was not performed for the ribosome footprinting samples. The samples were then column purified (RNA Clean & Concentrator 5, Zymo Research, catalog no. R1016) with the modifications that 2 volumes of RNA Binding Buffer and 4.5 volumes of ethanol were added to ribosome footprinting samples to purify small RNAs and 1 volume of RNA Binding Buffer and 1 volume of ethanol was added to total RNA samples to isolate RNA > 200 nt. Total RNA samples were then fragmented by partial alkaline hydrolysis. The samples were diluted to 100 µL with 5 mM Tris-HCl, pH 7.5 and incubated with 100 µL 2x alkaline fragmentation buffer (100 mM Na_2CO_3 pH 9.2, 2 mM EDTA) for 20 minutes at 95°C. The reaction was neutralized with 440 µL STOP Buffer (70 µL 3 M NaOAc pH 5.5, 2 µL Glycoblue, and 370 µL nuclease free water) and isopropanol precipitated overnight at -80°C.

Ribosome protected fragments and total RNA samples were then size selected by running the samples out on a 15% TBE-Urea polyacrylamide gel. Ribosome protected fragments were size selected between 28-nt and 34-nt as marked by RNA oligonucleotides oNTI199 and oNTI265, respectively*(27)*. Total RNA samples were size selected between 34-70 nt as marked by a 10 bp DNA ladder (Invitrogen, catalog no. 10821015). Gel slices were crushed and extracted at room temperature overnight in 400 µL RNA extraction buffer (300 mM NaOAc pH 5.5, 1 mM EDTA, 0.25% SDS) and isopropanol precipitated. Samples were then 3'dephosphorylated by denaturing at 65°C for 5 min and incubating with T4 PNK (NEB, catalog no. M0201S) in a 10 µL reaction (7 µL precipitated RNA, 1 µL 10x T4 PNK Buffer, 1 µL SUPERase Inhibitor, 1 µL 10 U/µL T4 PNK) at 37°C for 1 hour. The reaction was stopped through heat inactivation at 65°C for 20 min. To ligate adaptor, samples were then incubated with 0.5 µL of 50 µM Universal miRNA Cloning Linker (NEB, catalog no. S1315S) and denatured at 65°C for 5 min. The denatured sample was then incubated with 1 µL T4 RNA Ligase 2, truncated KQ (NEB, M0373S), 1 µL 10x buffer, 6 µL 50% PEG 8000, and 1.5 µL water for 4.5 h at 25°C. Free adaptor was then removed by addition of 1 µL 10 U/µL 5'-Deadenylase (NEB, M0331S). 1 µL 10 U/µL RecJ Exonuclease (Lucigen/Epicentre, RJ411250). and 1 µL 20 U/µL SUPERase Inhibitor. Samples were then purified using Zymo RNA Clean & Concentrator-5 columns using the protocol above to preserve small RNAs (100 µL sample, 200 µL RNA binding buffer, 450 µL 100% ethanol).

To perform reverse transcription, 10 µL sample was incubated with 2 µL of 1.25 µM RT primer (see table S2) and denatured at 65°C for 5 min. Reverse transcription (RT) was

performed with primers containing sample barcodes and unique molecular identifiers. RT was performed with SuperScript III (Thermo Fisher, 18080-044) in a 20 µL reaction (48°C, 40 min). RNA was then hydrolyzed by adding 2.2 µL of 1N NaOH and incubating for 20 min at 98°C. Samples were then purified using Zymo RNA Clean & Concentrator-5 columns (100 µL sample, 200 µL RNA binding buffer, 450 µL 100% ethanol). RT products were size selected and gel extracted from 10% TBE Urea polyacrylamide gels as described above instead that DNA extraction buffer was used for overnight extraction (300 mM NaCl, 10 mM Tris-HCl pH 8, 1 mM EDTA, 0.1% SDS). Eluate was then isopropanol precipitated overnight at -80°C overnight. Samples were then circularized with CircLigase (Illumina, CL4115K) in a 20 µL reaction (15 µL cDNA, 2 µL 10x CircLigase Buffer, 1 µL 1 mM ATP, 1 µL $MnCl_2$, 1 µL CircLigase) for 12 hours at 60°C and subsequently purified by Zymo RNA Clean & Concentrator 5 columns (100 µL sample, 200 µL RNA binding buffer, 450 µL 100% ethanol) and eluted with 12 µL 10 mM Tris-HCl pH 8. 1 µL of library was used for PCR amplification with Phusion High-Fidelity DNA Polymerase (Thermo Fisher, catalog no. F530S) (98°C 30s, 98°C 10s, 65°C 10s, 72°C 5s) for 9-10 cycles (see table S2 for primers). PCR product was PAGE purified from native 8% TBE polyacrylamide gels, extracted overnight using DNA extraction buffer, and isopropanol precipitated for > 2 h at -80°C. DNA was measured and quality controlled on the Agilent 2100 Bioanalyzer (High-Sensitivity DNA) by the Stanford Protein and Nucleic Acid (PAN) Facility. Libraries were sequenced by the Stanford Functional Genomics Facility (SFGF) on the Illumina NextSeq 500 (1x75nt).

Ribosome profiling analysis. For analysis pre-processing, UMI-tools*(53)* was used to extract sample barcodes and UMIs. Reads were demultiplexed, sample barcodes were removed, and reads were quality filtered (fastq_quality_filter -Q33 -q 20 -p 70) using FASTX-Toolkit (http://hannonlab.cshl.edu/fastx_toolkit/). The 3' adapter sequence CTGTAGGCACCATCAAT was removed using cutadapt*(54)*, and the 5' end of each read was then removed using fastx_trimmer from FASTX-Toolkit. To remove reads that aligned to rRNA, tRNA, and snRNAs, reads were first aligned to these sequences using bowtie2*(55)* (bowtie2 parameters: -L 18) and subsequently discarded. Filtered reads that did not align to rRNA/tRNA/snRNAs were then aligned using bowtie2 (bowtie2 parameters: --norc -L 18) to an GRCm38/mm10 transcriptome reference derived from UCSC/GENCODE VM20 knownCanonical annotations filtered for high confidence transcripts that contain at least one of the following: a Uniprot ID, a RefSeq ID, or an Entrez ID. PCR duplicates were then removed using UMI-tools. Ribosome protected fragments (RPFs) were then parsed for uniquely aligned reads, separated into read length

groups, and ribosome A site positions were determined by offsetting the distance of the 5' end of each read to canonical start sites in each length group and adding 4 nucleotides*(27)*. RNA-Seq reads were also parsed for uniquely aligned reads and were assigned to the center of each read. RPFs and RNA-Seq reads were then counted using the transcriptome annotations detailed above. Reads aligning to the CDS (with the first 15 codons and last 5 codons removed) were used for RPF libraries, and reads aligning to the entire transcript were used for RNA-Seq libraries. Transcripts with counts per million (cpm) > 0.75 for at least 3 ribosome profiling libraries were retained for downstream analysis. RPF and RNA-Seq libraries were then normalized separately by the method of trimmed mean of M-values (TMM) using edgeR*(56)*.

Differential translation analysis was performed using voom*(57)* and limma*(58)*. The following design matrix was constructed (~0 + genotype and type of library (RPF vs. RNA) + replicate batch + sex). The corresponding contrast matrix comparing translational efficiency (RPF - RNA) for each of the pairs of genotypes of interest (e.g., *Prx1*^{Cre}*;Rps6*$^{lox/+}$*;Trp53*$^{+/+}$ - *Prx1*^{Cre}*;Rps6*$^{lox/+}$*;Trp53*$^{+/+}$, *Prx1*^{Cre}*;Rps6*$^{lox/+}$*;Trp53*$^{-/-}$ - *Prx1*^{Cre}*;Rps6*$^{lox/+}$*;Trp53*$^{-/-}$, etc.) was also constructed. The data was then voom transformed to remove mean-variance count heteroscedascity. Using the design and contrast matrices mentioned above, linear models were fit to the data using limma with empirical Bayes moderation. Significant differentially translated genes were defined as those with FDR < 0.1 obtained using the Benjamini-Hochberg method.

Gene set enrichment analysis was performed using Camera *(59)* with mouse GO Biological Processes gene sets obtained from http://download.baderlab.org/EM_Genesets/current_release/Mouse/Entrezgene/. Gene sets were filtered such that all genes in gene sets have expression values in the dataset. Gene sets were also filtered to only include those with > 10 and < 500 genes. Enriched gene sets were visualized using Enrichment Map *(60)* and Cytoscape. For feature analyses, UTR RNA folding energies were obtained from UCSC Genome Browser (foldUtr5 and foldUtr3).

Samples and Statistical Analysis. All measurements were sampled from individual biological replicates. Replicates for mouse embryo experiments consisted of individual limbs, individual embryos, or pools of embryos if material was limiting. Experiments consisted of multiple embryos from multiple litters. Unless otherwise stated, when groups of continuous data are compared, two-tailed t-tests with unequal variance were performed. No statistical methods were used to predetermine sample size.

Code Availability. All custom codes are available upon request from the corresponding author.

Data Availability. Data that support the findings of this study have been deposited in the Gene Expression Omnibus under accession number GSE135722.

SUPPLEMENTARY TEXT

Mechanisms of p53 activation upon RP haploinsufficiency

Several mechanisms have been proposed to explain how RP haploinsufficiency can lead to p53 activation . Many studies support a mechanism in which a stoichiometrically unbalanced ribosome leads to the release of unincorporated RPs, mainly RPL5 and RPL11 *(22)*. RPL5/RPL11, which are also mutated in DBA, form the RPL5-RPL11-5SrRNA pre-ribosomal complex that inhibits the p53 suppressor and E3 ubiquitin ligase Mdm2, thus relieving Mdm2-mediated degradation of p53 *(6)*. Stabilization of p53 is thought to contribute, at least in part, to ribosomopathies through transcriptional activation of genes canonically involved in regulating cell proliferation and apoptosis *(6)*. Although the above model would predict that reduction in RPL5/RPL11 would not lead to activation of p53 as has been demonstrated in culture cells, p53 activation has indeed been observed in *in vivo* models upon depletion of Rpl11 *(7, 61)*. For example, in zebrafish, morpholino-mediated knockdown of Rpl11 led to the transcriptional upregulation of known p53-target genes *(61)*. Transcriptional upregulation of known p53-target genes *Cdkn1a* and *Bax* was also observed *in vivo* in mice upon haploinsufficiency of Rpl11, although the p53 response appeared blunted in immortalized mouse embryonic fibroblasts derived from these mice *(7)*. These studies highlight the importance of studying RP haploinsufficiency in *in vivo* contexts as p53-responsiveness to RP haploinsufficiency may differ between intact organisms and immortalized cell lines.

SUPPLEMENTARY TABLES

Supplementary Table 1. Limb phenotype quantification

Supplementary Table 2. Primers and oligos

Supplementary Table 3. Ribosome profiling results from *Prx1*^{Cre}*;Rps6*$^{lox/+}$ vs. *Rps6*$^{lox/+}$ E10.5 limbs

Supplementary Table 4. Ribosome profiling results from *Prx1*^{Cre}*;Rps6*$^{lox/+}$*;Trp53*$^{-/-}$ vs. *Rps6*$^{lox/+}$*;Trp53*$^{-/-}$ E10.5 limbs

Supplementary Table 5. Gene set enrichment analysis of translational efficiency changes in *Prx1*^{Cre}*;Rps6*$^{lox/+}$ vs. *Rps6*$^{lox/+}$ E10.5 limbs

Supplementary Table 6. RNA folding energies and lengths of transcripts.

FIGURE LEGENDS

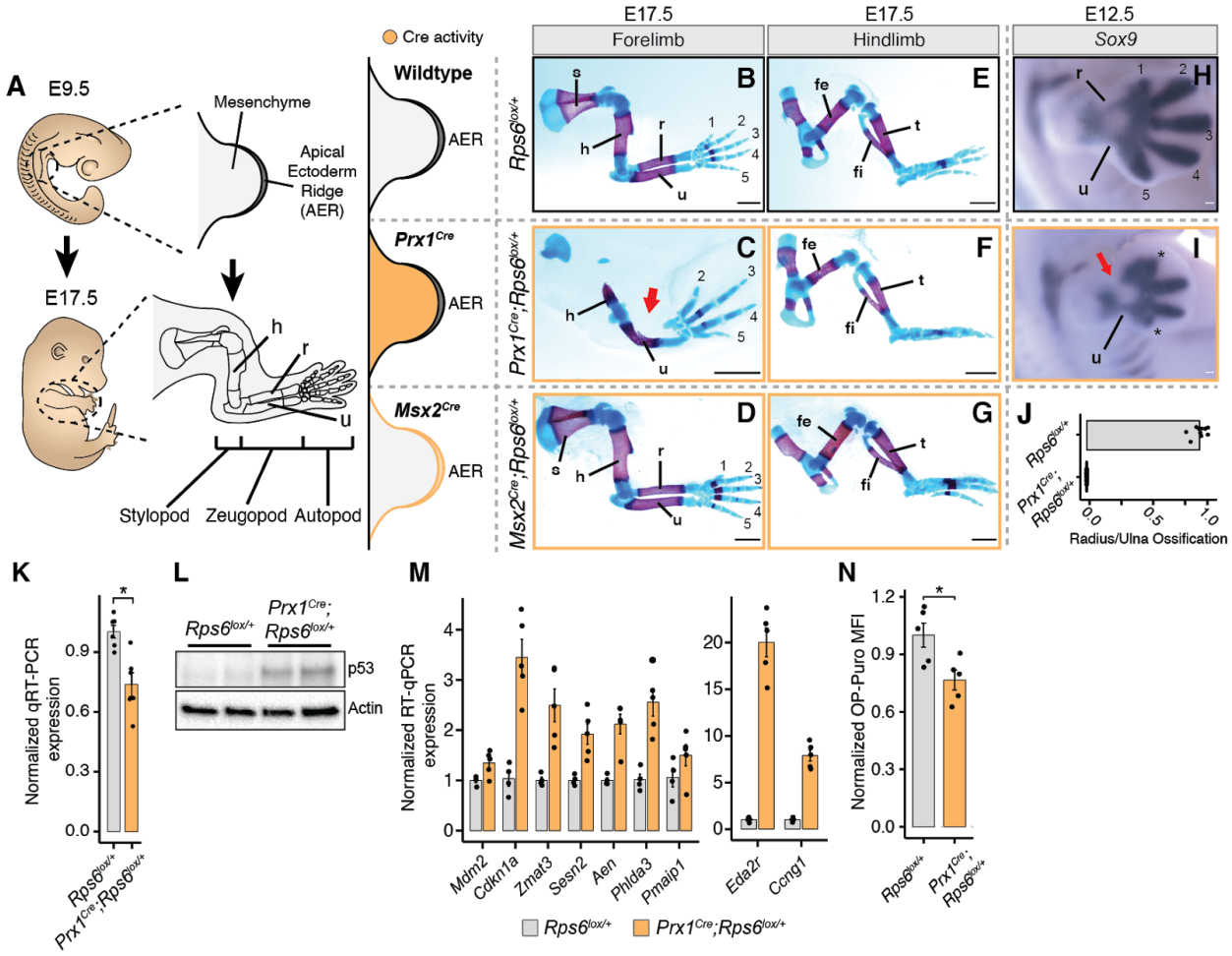

Fig. 1. *Rps6* haploinsufficiency in the developing limb bud mesenchyme leads to selective patterning defects marked by activation of p53 and a reduction in global protein synthesis. (**A**) Overview of forelimb development from embryonic day 9.5 (E9.5) to E17.5. Schematic illustrating *Prx1*^{Cre} expression in limb bud mesenchyme (orange) and *Msx2*^{Cre} expression in the overlying AER (green). AER, apical ectodermal ridge; h, humerus; r, radius; u, ulna. (**B-G**)**,** Representative images of E17.5 forelimbs and hindlimbs. Bone, red; Cartilage, blue. Numbers indicate digits. Arrow indicates absence of radius. Scale bars, 1 mm. (**H-I**) *Sox9 in situ* hybridization of E12.5 forelimbs. Numbers indicate mesenchymal condensations leading to digit formation. *Impaired digit development. Arrow indicates absence of radius. Scale bars, 0.1 mm. (**J**) Radius ossification normalized to ulna ossification in E17.5 forelimbs. *n* = 10 limbs (*Rps6*$^{lox/+}$), *n* = 28 limbs (*Prx1*^{Cre}*;Rps6*$^{lox/+}$). (**K**) RT-qPCR of *Rps6* mRNA in forelimbs from E10.5 embryos. Expression normalized to the geometric mean of *Actb, Tbp, Ubb, Exo5, Pkm2,* and *Nadk2* then to wildtype values. n = 6. (**L**) Representative Western blot of p53 in E10.5 forelimbs. (**M**) RT-qPCR of p53 target genes in E10.5 forelimbs. Expression was normalized to *Actb* and to the mean of wildtype values.

n = 4 embryos (*Rps6*$^{lox/+}$), *n* = 5 embryos (*Prx1*^{Cre}*;Rps6*$^{lox/+}$). (**N**) OP-Puro MFI of cells dissociated from E10.5 forelimbs normalized to wildtype. *n* = 5 embryos; MFI = median fluorescence intensity. For all bar plots, error bars = SEM, * $P < 0.05$, ** $P < 0.01$, *** $P < 0.001$, **** $P < 0.0001$, two-tailed t-test, unequal variance.

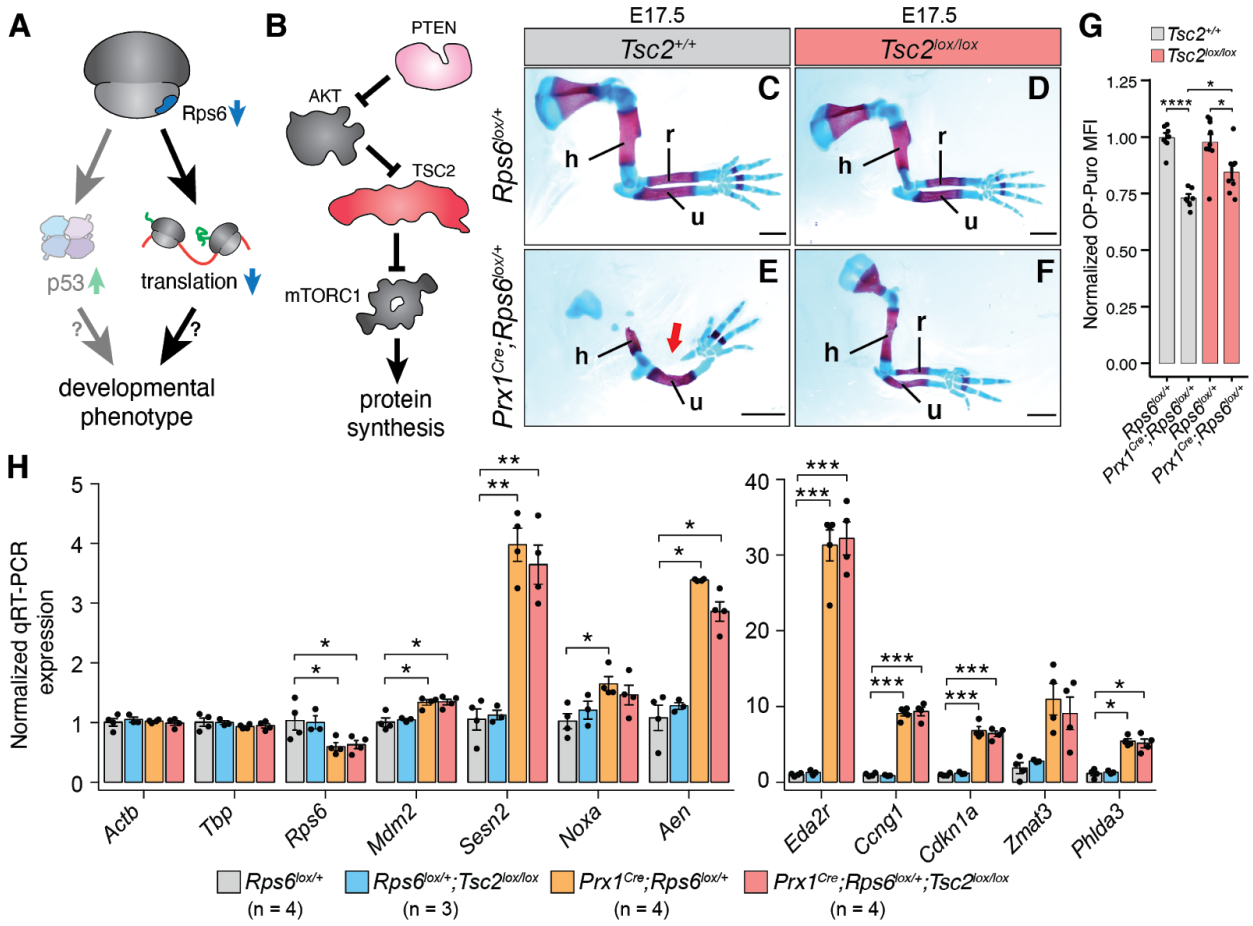

Fig. 2. mTORC1 activation and corresponding augmented protein synthesis rescues phenotypes associated with Rps6 haploinsufficiency. (**A**) Overview of pathways potentially leading to developmental phenotypes upon *Rps6* haploinsufficiency. (**B**) Schematic of mTORC1 regulation and downstream effects. (**C-F**) Representative E17.5 forelimbs and hindlimbs of wildtype (*Rps6*$^{lox/+}$) and *Prx1*^{Cre}*;Rps6*$^{lox/+}$ embryos in a *Tsc2*^{lox} background. Arrow indicates absence of radius. Scale bars, 1 mm; h, humerus; r, radius; u, ulna. (**G**) OP-Puro MFI of cells dissociated from E10.5 forelimbs normalized to wildtype. *n* = 7 embryos, (*Rps6*$^{lox/+}$*;Tsc2*$^{+/+}$); *n* = 6 embryos, (*Prx1*^{Cre}*;Rps6*$^{lox/+}$*;Tsc2*$^{+/+}$); *n* = 9 embryos, (*Rps6*$^{lox/+}$*;Tsc2*$^{lox/lox}$); *n* = 8 embryos, (*Prx1*^{Cre}*;Rps6*$^{lox/+}$*;Tsc2*$^{lox/lox}$).

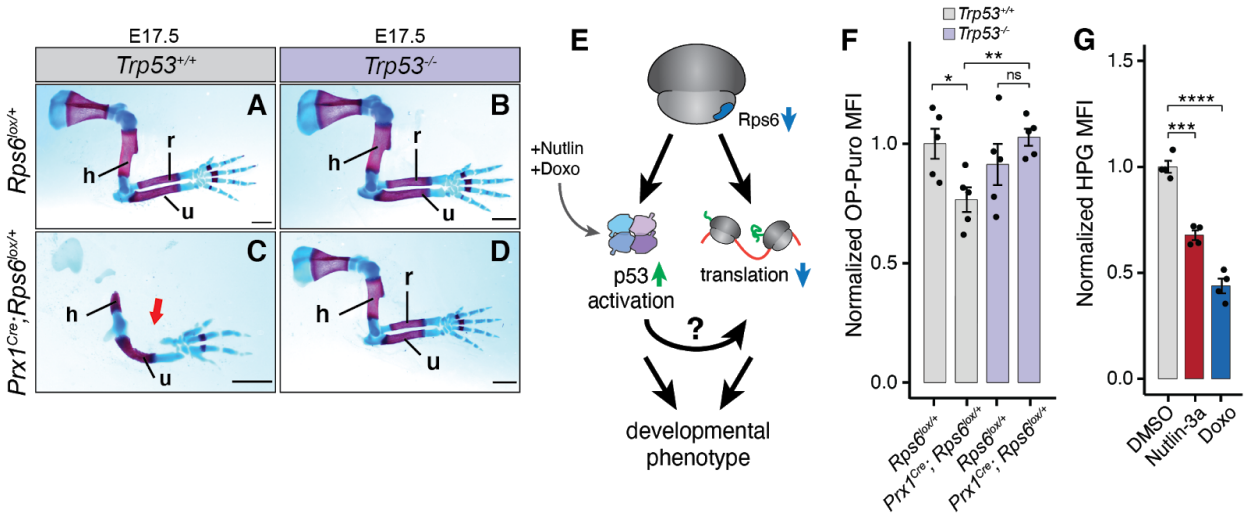

Fig. 3. Loss of p53 rescues the *Rps6* haploinsufficiency phenotypes and p53 activation mediates translational changes upon Rps6 reduction. (**A-D**) Representative E17.5 forelimbs and hindlimbs of wildtype and *Prx1*^{Cre};*Rps6*$^{lox/+}$ embryos in a *Trp53*$^{-}$ background. Arrow indicates absence of radius. Scale bars, 1 mm; h, humerus; r, radius; u, ulna. (**E**) Potential pathways for p53-dependent translational control upon *Rps6* haploinsufficiency. (**F**) OP-Puro MFI of cells dissociated from E10.5 forelimbs normalized to wildtype. n = 5 embryos. (**G**) HPG MFI of MEFs treated with Nutlin-3a or doxorubicin normalized to mean of DMSO treated control. 8 h treatment, n = 4. For all bar plots, error bars = SEM, * $P < 0.05$, ** $P < 0.01$, *** $P < 0.001$, **** $P < 0.0001$, two-tailed t-test, unequal variance.

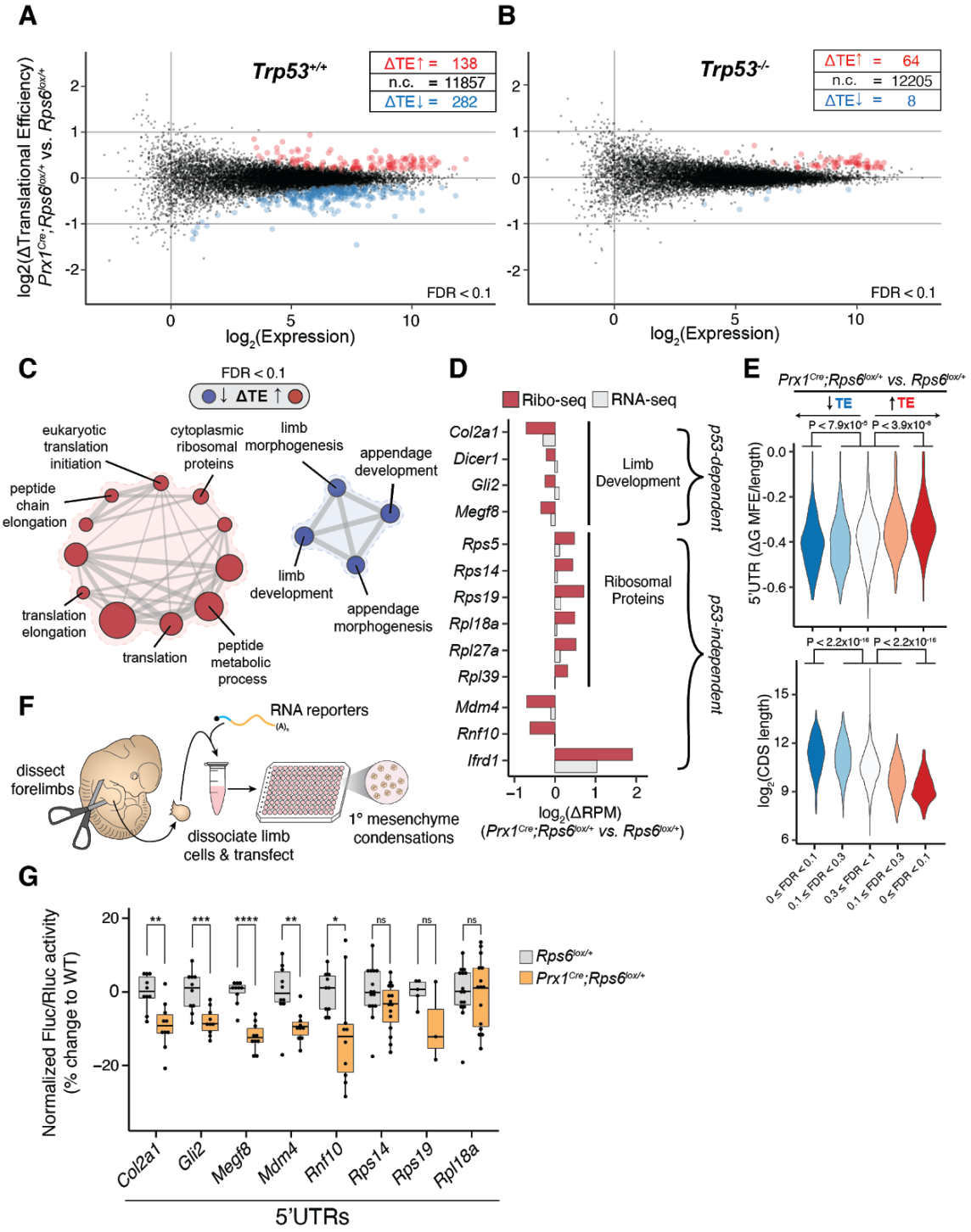

Fig. 4. *In vivo* ribosome profiling reveals the landscape of p53-dependent and -independent translation changes upon Rps6 reduction. (**A-B**) MA plot of change in translational efficiency (ΔTE) in E10.5 *Prx1*^{Cre}*;Rps6*$^{lox/+}$ vs. *Rps6*$^{lox/+}$ embryonic forelimbs in *Trp53*$^{+/+}$ background (**A**) and *Trp53*$^{-/-}$ background (**B**). red, ΔTE > 0; blue, ΔTE < 0; *n* = 3 biological replicates (2 embryos each); FDR < 0.1. (**C**)

Gene sets enriched for transcripts changing in TE in E10.5 *Prx1*^{Cre}*;Rps6*$^{lox/+}$ vs. *Rps6*$^{lox/+}$ forelimbs. Analysis performed by CAMERA, transcripts filtered for expressed genes; node size, gene set size; edge size, gene set overlap; red, ΔTE > 0; blue, ΔTE < 0; FDR < 0.1. (**D**) Relative change in ribosome footprints for select high-confidence transcripts (red; FDR < 0.1). Relative changes in mRNA expression shown in grey. (**E**) Violin plots quantifying ΔTE relative to 5'UTR structuredness as predicted by UCSC genome browser foldUtr5 normalized to UTR length (ΔG MFE / 5'UTR length) and relative to CDS length. Transcripts are stratified by direction of ΔTE (blue, down; red, up) and FDR ($0 \leq$ FDR < 0.1, $0.1 \leq$ FDR < 0.3, $0.3 \leq$ FDR ≤ 1); Mann-Whitney U test. (**F**) Workflow of the primary limb micromass assay. (**G**) Firefly/Renilla luciferase activity from transfection of RNA reporters in E11.5 limb micromass assays normalized to the geometric mean of *Pkm* and *Cnot10* 5'UTR activities and wildtype. For box-plots, center line, median; box limits, first and third quartiles; whiskers, 1.5x interquartile range; points, outliers. * $P < 0.05$, ** $P < 0.01$, *** $P < 0.001$, **** $P < 0.0001$, two-tailed t-test, unequal variance.

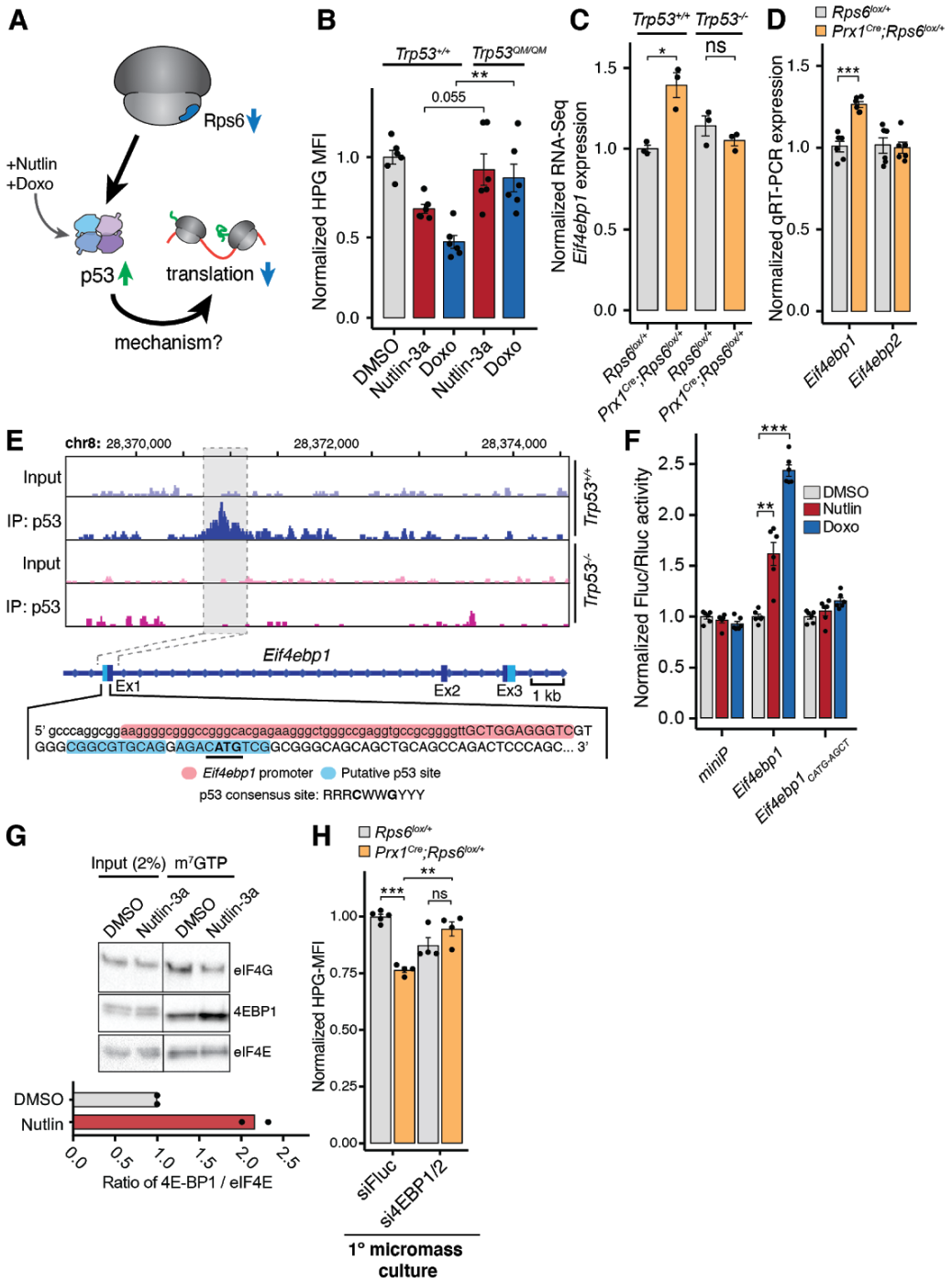

Fig. 5. p53 controls translation via transcriptional upregulation of *Eif4ebp1*. (**A**) Potential pathways of p53-dependent translational control. (**B**) HPG MFI of MEFs expressing wildtype or transactivation dead p53 (*Trp53*^{QM}) treated with Nutlin-3a or doxorubicin normalized to mean of DMSO control expressing wildtype p53. 8 h treatment, n = 6. (**C**) *Eif4ebp1* expression from RNA-Seq of E10.5 forelimbs

normalized to wildtype (*Rps6*$^{lox/+}$*;Trp53*$^{+/+}$), *n* = 3. (**D**) RT-qPCR of *Eif4ebp1* and *Eif4ebp2* from E10.5 forelimbs normalized to the geometric mean of housekeeping genes (*Actb, Tbp, Ubb, Exo5, Pkm2, Nadk2*) and wildtype (*Rps6*$^{lox/+}$*;Trp53*$^{+/+}$), *n* = 6. (**E**) p53 ChIP-Seq gene track of *Eif4ebp1* locus *(36)*. Transcription start site denoted by capital letters with the *Eif4ebp1* promoter highlighted (red). Putative p53-binding region is highlighted (blue) with the *Eif4ebp1* start codon bolded and p53 core binding sequence is underlined. (**F**) Quantification of Firefly luciferase activity normalized to Renilla luciferase transfection control then to DMSO control of each construct. Plasmid containing either a minimal promoter, the *Eif4ebp1* region, or mutated *Eif4ebp1* region (see fig. S14E) were transfected into NIH3T3 cells. Cells were treated with DMSO, Nutlin-3a, or doxorubicin for 8 h; *n* = 6. (**G**) Representative cap-binding assay of NIH3T3 cells treated with Nutlin-3a for 8 h. Bottom: ratio of 4E-BP1 to eIF4E in cap-binding assays; *n* = *2*. (**H**) HPG MFI upon siRNA treatment in primary limb micromass cultures from E10.5 forelimbs. Values normalized to wildtype and control siRNA; *n* = 4. For all bar plots, error bars = SEM, * $P < 0.05$, ** $P < 0.01$, *** $P < 0.001$, **** $P < 0.0001$, two-tailed t-test, unequal variance.

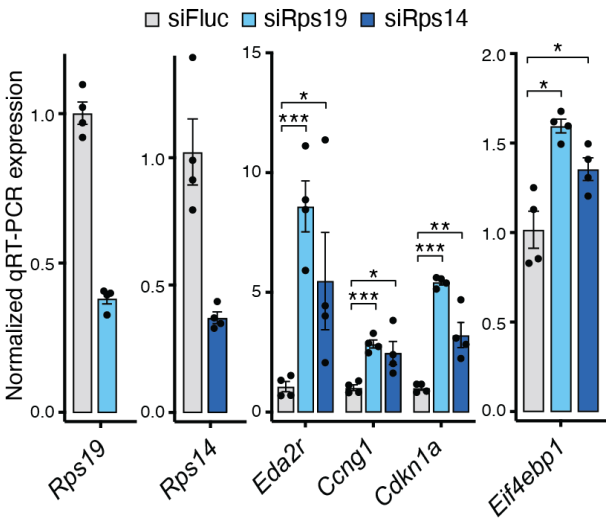

Fig. 6. Depletion of ribosomal proteins commonly mutated in ribosomopathies induces *Eif4ebp1* expression. Relative mRNA expression of p53 target genes and ribosomal proteins in primary limb micromass cultures after siRNA knockdown of Rps14, Rps19. Expression was normalized to the geometric mean of *TBP* and *NupL1* and then to siRNA control. $n = 4$. For all bar plots, error bars = SEM, * $P < 0.05$, ** $P < 0.01$, *** $P < 0.001$, **** $P < 0.0001$, two-tailed t-test, unequal variance.

ACKNOWLEDGMENTS

The authors would like to thank Kotaro Fujii (Stanford), Katrina Cabaltera, Jing Huang (Stanford), Naomi Genuth (Stanford), and David Mahoney (Stanford) for their experimental contributions as well as the Stanford FACS facility. The authors would also like to thank George Thomas (IDIBELL) for generously providing the *Rps6*^{lox} mice, and members of the Barna lab for critical feedback and discussion. **Funding:** Supported by New York Stem Cell Foundation grant NYSCF-R-I36 (M.B.), New York Stem Cell Robertson Investigator (M.B.), NIH grant 1R01HD086634 (M.B.), Alfred P. Sloan Research Fellowship (M.B.), Pew Scholars Award (M.B.), NIH grant R35CA242986 (D.R.), March of Dimes Foundation grant no. 6-FY15-189 (L.D.A.), NIH R35 grant CA197591 (L.D.A.), Paul and Daisy Soros Fellowships for New Americans (G.C.T), Stanford Medical Scientist Training Program (G.C.T.), Canadian Institutes for Health Research Fellowship (C.H.K. and O.Z.), Stanford Dean's Fellowship (C.H.K.), Helen Hay Whitney Foundation Fellowship (O.Z.), NIH/NIDDK grant K08DK119561 (C.M.F.), National Institutes of Health Developmental Biology Training Grant 5T32GM007790-41 (H.D.R.), Campini Foundation and the University of California, San Francisco, Department of Pediatrics K12 (Award 5K12HDO72222-05) (C.M.F.), and the Jane Coffin Childs Fund Postdoctoral Fellowship (M.E.B.). **Author Contributions:** M.B. and G.C.T. conceived, and M.B. supervised the project; G.C.T., C.H.K., and M.B. designed the experiments; G.C.T., P.S.K., H.D.R., M.E.B., L.S., and O.Z. performed mouse embryo experiments and phenotyping; C.H.K. performed cell culture experiments; G.C.T., C.H.K., C.M.F., and N.R. performed metabolic labeling experiments; G.C.T. performed and analyzed ribosome profiling experiments; G.C.T. and C.H.K. performed RT-qPCR experiments; C.H.K. performed Western blotting experiments and reporter assays; N.R., M.E.B., and L.D.A. guided experiments related to p53; C.M.F. and D.R. guided experiments related to OP-Puro labeling and characterization of global protein synthesis changes ; G.C.T. and C.H.K. performed the rest of the experiments; M.B., G.C.T., and C.H.K. wrote the manuscript with input from all the authors. **Competing Interests:** The authors declare no competing interests. **Data and materials availability:** All data are available in the manuscript or the supplementary materials. Data that support the findings of this study have been deposited in the Gene Expression Omnibus under accession number GSE135722.

REFERENCES

1. P. C. Yelick, P. A. Trainor, Ribosomopathies: Global process, tissue specific defects., *Rare Dis.* **3**, e1025185 (2015).

2. C. Clinton, H. T. Gazda, in *GeneReviews(®)*, R. A. Pagon, M. P. Adam, H. H. Ardinger, S. E. Wallace, A. Amemiya, L. J. Bean, T. D. Bird, C.-T. Fong, H. C. Mefford, R. J. Smith, K. Stephens, R. A. Pagon, M. P. Adam, H. H. Ardinger, S. E. Wallace, A. Amemiya, L. J. Bean, T. D. Bird, C.-T. Fong, H. C. Mefford, R. J. Smith, K. Stephens, R. A. Pagon, M. P. Adam, H. H. Ardinger, S. E. Wallace, A. Amemiya, L. J. Bean, T. D. Bird, C.-T. Fong, H. C. Mefford, R. J. Smith, K. Stephens, R. A. Pagon, M. P. Adam, H. H. Ardinger, S. E. Wallace, A. Amemiya, L. J. Bean, T. D. Bird, C.-T. Fong, H. C. Mefford, R. J. Smith, K. Stephens, R. A. Pagon, M. P. Adam, H. H. Ardinger, S. E. Wallace, A. Amemiya, L. J. Bean, T. D. Bird, C.-T. Fong, H. C. Mefford, R. J. Smith, K. Stephens, Eds. (University of Washington, Seattle, Seattle (WA), 1993).

3. R. K. Khajuria, M. Munschauer, J. C. Ulirsch, C. Fiorini, L. S. Ludwig, S. K. McFarland, N. J. Abdulhay, H. Specht, H. Keshishian, D. R. Mani, M. Jovanovic, S. R. Ellis, C. P. Fulco, J. M. Engreitz, S. Schütz, J. Lian, K. W. Gripp, O. K. Weinberg, G. S. Pinkus, L. Gehrke, V. G. Sankaran, Ribosome levels selectively regulate translation and lineage commitment in human hematopoiesis., *Cell* **173**, 90-103.e19 (2018).

4. S. Dutt, A. Narla, K. Lin, A. Mullally, N. Abayasekara, C. Megerdichian, F. H. Wilson, T. Currie, A. Khanna-Gupta, N. Berliner, J. L. Kutok, B. L. Ebert, Haploinsufficiency for ribosomal protein genes causes selective activation of p53 in human erythroid progenitor cells., *Blood* **117**, 2567–2576 (2011).

5. A. Narla, B. L. Ebert, Ribosomopathies: human disorders of ribosome dysfunction., *Blood* **115**, 3196–3205 (2010).

6. C. Deisenroth, Y. Zhang, Ribosome biogenesis surveillance: probing the ribosomal protein-Mdm2-p53 pathway., *Oncogene* **29**, 4253–4260 (2010).

7. L. Morgado-Palacin, G. Varetti, S. Llanos, G. Gómez-López, D. Martinez, M. Serrano, Partial Loss of Rpl11 in Adult Mice Recapitulates Diamond-Blackfan Anemia and Promotes Lymphomagenesis., *Cell Rep.* **13**, 712–722 (2015).

8. S. Volarevic, M. J. Stewart, B. Ledermann, F. Zilberman, L. Terracciano, E. Montini, M. Grompe, S. C. Kozma, G. Thomas, Proliferation, but not growth, blocked by conditional deletion of 40S ribosomal protein S6., *Science* **288**, 2045–2047 (2000).

9. L. Panić, S. Tamarut, M. Sticker-Jantscheff, M. Barkić, D. Solter, M. Uzelac, K. Grabusić, S. Volarević, Ribosomal protein S6 gene haploinsufficiency is associated with activation of a p53-dependent checkpoint during gastrulation., *Mol. Cell. Biol.* **26**, 8880–8891 (2006).

10. K. A. McGowan, W. W. Pang, R. Bhardwaj, M. G. Perez, J. V. Pluvinage, B. E. Glader, R. Malek, S. M. Mendrysa, I. L. Weissman, C. Y. Park, G. S. Barsh, Reduced ribosomal protein gene dosage and p53 activation in low-risk myelodysplastic syndrome., *Blood* **118**, 3622–3633 (2011).

11. H. T. Gazda, M. R. Sheen, A. Vlachos, V. Choesmel, M.-F. O'Donohue, H. Schneider, N. Darras, C. Hasman, C. A. Sieff, P. E. Newburger, S. E. Ball, E. Niewiadomska, M. Matysiak, J. M. Zaucha, B. Glader, C. Niemeyer, J. J. Meerpohl, E. Atsidaftos, J. M. Lipton, P.-E. Gleizes, A. H. Beggs, Ribosomal protein L5 and L11 mutations are associated with cleft palate and abnormal thumbs in Diamond-Blackfan anemia patients., *Am. J. Hum. Genet.* **83**, 769–780 (2008).

12. R. Zeller, J. López-Ríos, A. Zuniga, Vertebrate limb bud development: moving towards integrative

analysis of organogenesis., *Nat. Rev. Genet.* **10**, 845–858 (2009).

13. M. Logan, J. F. Martin, A. Nagy, C. Lobe, E. N. Olson, C. J. Tabin, Expression of Cre Recombinase in the developing mouse limb bud driven by a Prxl enhancer., *Genesis* **33**, 77–80 (2002).

14. X. Sun, M. Lewandoski, E. N. Meyers, Y. H. Liu, R. E. Maxson, G. R. Martin, Conditional inactivation of Fgf4 reveals complexity of signalling during limb bud development., *Nat. Genet.* **25**, 83–86 (2000).

15. J. A. Hurst, M. Baraitser, B. Wonke, Autosomal dominant transmission of congenital erythroid hypoplastic anemia with radial abnormalities., *Am. J. Med. Genet.* **40**, 482–484 (1991).

16. M. E. Bowen, J. McClendon, H. K. Long, A. Sorayya, J. L. Van Nostrand, J. Wysocka, L. D. Attardi, The Spatiotemporal Pattern and Intensity of p53 Activation Dictates Phenotypic Diversity in p53-Driven Developmental Syndromes., *Dev. Cell* (2019), doi:10.1016/j.devcel.2019.05.015.

17. C. A. Brady, D. Jiang, S. S. Mello, T. M. Johnson, L. A. Jarvis, M. M. Kozak, D. Kenzelmann Broz, S. Basak, E. J. Park, M. E. McLaughlin, A. N. Karnezis, L. D. Attardi, Distinct p53 transcriptional programs dictate acute DNA-damage responses and tumor suppression., *Cell* **145**, 571–583 (2011).

18. R. A. J. Signer, J. A. Magee, A. Salic, S. J. Morrison, Haematopoietic stem cells require a highly regulated protein synthesis rate., *Nature* **509**, 49–54 (2014).

19. R. A. Saxton, D. M. Sabatini, mTOR Signaling in Growth, Metabolism, and Disease., *Cell* **168**, 960–976 (2017).

20. Y. Zhang, J. Nicholatos, J. R. Dreier, S. J. H. Ricoult, S. B. Widenmaier, G. S. Hotamisligil, D. J. Kwiatkowski, B. D. Manning, Coordinated regulation of protein synthesis and degradation by mTORC1., *Nature* **513**, 440–443 (2014).

21. A. Garami, F. J. T. Zwartkruis, T. Nobukuni, M. Joaquin, M. Roccio, H. Stocker, S. C. Kozma, E. Hafen, J. L. Bos, G. Thomas, Insulin activation of Rheb, a mediator of mTOR/S6K/4E-BP signaling, is inhibited by TSC1 and 2., *Mol. Cell* **11**, 1457–1466 (2003).

22. J. Kasteri, D. Das, X. Zhong, L. Persaud, A. Francis, H. Muharam, M. Sauane, Translation Control by p53., *Cancers (Basel)* **10** (2018), doi:10.3390/cancers10050133.

23. A. V. Budanov, M. Karin, p53 target genes sestrin1 and sestrin2 connect genotoxic stress and mTOR signaling., *Cell* **134**, 451–460 (2008).

24. F. Loayza-Puch, J. Drost, K. Rooijers, R. Lopes, R. Elkon, R. Agami, p53 induces transcriptional and translational programs to suppress cell proliferation and growth., *Genome Biol.* **14**, R32 (2013).

25. S. Wang, E. A. Konorev, S. Kotamraju, J. Joseph, S. Kalivendi, B. Kalyanaraman, Doxorubicin induces apoptosis in normal and tumor cells via distinctly different mechanisms. intermediacy of H(2)O(2)- and p53-dependent pathways., *J. Biol. Chem.* **279**, 25535–25543 (2004).

26. L. T. Vassilev, B. T. Vu, B. Graves, D. Carvajal, F. Podlaski, Z. Filipovic, N. Kong, U. Kammlott, C. Lukacs, C. Klein, N. Fotouhi, E. A. Liu, In vivo activation of the p53 pathway by small-molecule antagonists of MDM2., *Science* **303**, 844–848 (2004).

27. N. T. Ingolia, L. F. Lareau, J. S. Weissman, Ribosome profiling of mouse embryonic stem cells reveals the complexity and dynamics of mammalian proteomes., *Cell* **147**, 789–802 (2011).

28. N. J. McGlincy, N. T. Ingolia, Transcriptome-wide measurement of translation by ribosome profiling., *Methods* **126**, 112–129 (2017).

29. B. Lee, H. Vissing, F. Ramirez, D. Rogers, D. Rimoin, Identification of the molecular defect in a family

with spondyloepiphyseal dysplasia., *Science* **244**, 978–980 (1989).

30. B. D. Harfe, M. T. McManus, J. H. Mansfield, E. Hornstein, C. J. Tabin, The RNaseIII enzyme Dicer is required for morphogenesis but not patterning of the vertebrate limb., *Proc Natl Acad Sci USA* **102**, 10898–10903 (2005).

31. R. Mo, A. M. Freer, D. L. Zinyk, M. A. Crackower, J. Michaud, H. H. Heng, K. W. Chik, X. M. Shi, L. C. Tsui, S. H. Cheng, A. L. Joyner, C. Hui, Specific and redundant functions of Gli2 and Gli3 zinc finger genes in skeletal patterning and development., *Development* **124**, 113–123 (1997).

32. S. R. F. Twigg, D. Lloyd, D. Jenkins, N. E. Elçioglu, C. D. O. Cooper, N. Al-Sannaa, A. Annagür, G. Gillessen-Kaesbach, I. Hüning, S. J. L. Knight, J. A. Goodship, B. D. Keavney, P. L. Beales, O. Gileadi, S. J. McGowan, A. O. M. Wilkie, Mutations in multidomain protein MEGF8 identify a Carpenter syndrome subtype associated with defective lateralization., *Am. J. Hum. Genet.* **91**, 897–905 (2012).

33. J.-C. W. Marine, M. A. Dyer, A. G. Jochemsen, MDMX: from bench to bedside., *J. Cell Sci.* **120**, 371–378 (2007).

34. D. E. Weinberg, P. Shah, S. W. Eichhorn, J. A. Hussmann, J. B. Plotkin, D. P. Bartel, Improved Ribosome-Footprint and mRNA Measurements Provide Insights into Dynamics and Regulation of Yeast Translation., *Cell Rep.* **14**, 1787–1799 (2016).

35. M. Barna, L. Niswander, Visualization of cartilage formation: insight into cellular properties of skeletal progenitors and chondrodysplasia syndromes., *Dev. Cell* **12**, 931–941 (2007).

36. D. Kenzelmann Broz, S. Spano Mello, K. T. Bieging, D. Jiang, R. L. Dusek, C. A. Brady, A. Sidow, L. D. Attardi, Global genomic profiling reveals an extensive p53-regulated autophagy program contributing to key p53 responses., *Genes Dev.* **27**, 1016–1031 (2013).

37. J. Pelletier, J. Graff, D. Ruggero, N. Sonenberg, Targeting the eIF4F translation initiation complex: a critical nexus for cancer development., *Cancer Res.* **75**, 250–263 (2015).

38. M. L. Truitt, C. S. Conn, Z. Shi, X. Pang, T. Tokuyasu, A. M. Coady, Y. Seo, M. Barna, D. Ruggero, Differential Requirements for eIF4E Dose in Normal Development and Cancer., *Cell* **162**, 59–71 (2015).

39. C. Bi, X. Zhang, T. Lu, X. Zhang, X. Wang, B. Meng, H. Zhang, P. Wang, J. M. Vose, W. C. Chan, T. W. McKeithan, K. Fu, Inhibition of 4EBP phosphorylation mediates the cytotoxic effect of mechanistic target of rapamycin kinase inhibitors in aggressive B-cell lymphomas., *Haematologica* **102**, 755–764 (2017).

40. M. Ding, T. H. Van der Kwast, R. N. Vellanki, W. D. Foltz, T. D. McKee, N. Sonenberg, P. P. Pandolfi, M. Koritzinsky, B. G. Wouters, The mTOR Targets 4E-BP1/2 Restrain Tumor Growth and Promote Hypoxia Tolerance in PTEN-driven Prostate Cancer., *Mol. Cancer Res.* **16**, 682–695 (2018).

41. G. J. Brunn, C. C. Hudson, A. Sekulić, J. M. Williams, H. Hosoi, P. J. Houghton, J. C. Lawrence, R. T. Abraham, Phosphorylation of the translational repressor PHAS-I by the mammalian target of rapamycin., *Science* **277**, 99–101 (1997).

42. N. Robichaud, N. Sonenberg, D. Ruggero, R. J. Schneider, Translational control in cancer., *Cold Spring Harb. Perspect. Biol.* **11** (2019), doi:10.1101/cshperspect.a032896.

43. A. Vlachos, P. S. Rosenberg, E. Atsidaftos, B. P. Alter, J. M. Lipton, Incidence of neoplasia in Diamond Blackfan anemia: a report from the Diamond Blackfan Anemia Registry., *Blood* **119**, 3815–3819 (2012).

44. M. Groszer, R. Erickson, D. D. Scripture-Adams, R. Lesche, A. Trumpp, J. A. Zack, H. I. Kornblum, X.

Liu, H. Wu, Negative regulation of neural stem/progenitor cell proliferation by the Pten tumor suppressor gene in vivo., *Science* **294**, 2186–2189 (2001).

45. O. Hernandez, S. Way, J. McKenna, M. J. Gambello, Generation of a conditional disruption of the Tsc2 gene., *Genesis* **45**, 101–106 (2007).

46. T. Jacks, L. Remington, B. O. Williams, E. M. Schmitt, S. Halachmi, R. T. Bronson, R. A. Weinberg, Tumor spectrum analysis in p53-mutant mice., *Curr. Biol.* **4**, 1–7 (1994).

47. A. O. Perantoni, O. Timofeeva, F. Naillat, C. Richman, S. Pajni-Underwood, C. Wilson, S. Vainio, L. F. Dove, M. Lewandoski, Inactivation of FGF8 in early mesoderm reveals an essential role in kidney development., *Development* **132**, 3859–3871 (2005).

48. M. D. Muzumdar, B. Tasic, K. Miyamichi, L. Li, L. Luo, A global double-fluorescent Cre reporter mouse., *Genesis* **45**, 593–605 (2007).

49. T. Lufkin, In situ hybridization of whole-mount mouse embryos with RNA probes: hybridization, washes, and histochemistry., *CSH Protoc.* **2007**, pdb.prot4823 (2007).

50. N. T. Ingolia, G. A. Brar, S. Rouskin, A. M. McGeachy, J. S. Weissman, The ribosome profiling strategy for monitoring translation in vivo by deep sequencing of ribosome-protected mRNA fragments., *Nat. Protoc.* **7**, 1534–1550 (2012).

51. C. Cenik, E. S. Cenik, G. W. Byeon, F. Grubert, S. I. Candille, D. Spacek, B. Alsallakh, H. Tilgner, C. L. Araya, H. Tang, E. Ricci, M. P. Snyder, Integrative analysis of RNA, translation, and protein levels reveals distinct regulatory variation across humans., *Genome Res.* **25**, 1610–1621 (2015).

52. R. A. Flynn, L. Martin, R. C. Spitale, B. T. Do, S. M. Sagan, B. Zarnegar, K. Qu, P. A. Khavari, S. R. Quake, P. Sarnow, H. Y. Chang, Dissecting noncoding and pathogen RNA-protein interactomes., *RNA* **21**, 135–143 (2015).

53. T. Smith, A. Heger, I. Sudbery, UMI-tools: modeling sequencing errors in Unique Molecular Identifiers to improve quantification accuracy., *Genome Res.* **27**, 491–499 (2017).

54. M. Martin, Cutadapt removes adapter sequences from high-throughput sequencing reads, *EMBnet j.* **17**, 10 (2011).

55. B. Langmead, S. L. Salzberg, Fast gapped-read alignment with Bowtie 2., *Nat. Methods* **9**, 357–359 (2012).

56. M. D. Robinson, D. J. McCarthy, G. K. Smyth, edgeR: a Bioconductor package for differential expression analysis of digital gene expression data., *Bioinformatics* **26**, 139–140 (2010).

57. C. W. Law, Y. Chen, W. Shi, G. K. Smyth, voom: Precision weights unlock linear model analysis tools for RNA-seq read counts., *Genome Biol.* **15**, R29 (2014).

58. M. E. Ritchie, B. Phipson, D. Wu, Y. Hu, C. W. Law, W. Shi, G. K. Smyth, limma powers differential expression analyses for RNA-sequencing and microarray studies., *Nucleic Acids Res.* **43**, e47 (2015).

59. D. Wu, G. K. Smyth, Camera: a competitive gene set test accounting for inter-gene correlation., *Nucleic Acids Res.* **40**, e133 (2012).

60. D. Merico, R. Isserlin, O. Stueker, A. Emili, G. D. Bader, Enrichment map: a network-based method for gene-set enrichment visualization and interpretation., *PLoS ONE* **5**, e13984 (2010).

61. N. Danilova, K. M. Sakamoto, S. Lin, Ribosomal protein L11 mutation in zebrafish leads to

haematopoietic and metabolic defects., *Br. J. Haematol.* **152**, 217–228 (2011).